

Large gyro-orbit model of ion velocity distribution in plasma near a wall in a grazing-angle magnetic field

Alessandro Geraldini^{1†}

¹Institute for Research in Electronics and Applied Physics, University of Maryland, College Park, MD 20740, USA

(Received xx; revised xx; accepted xx)

A model is presented for the ion distribution function in a plasma at a solid target with a magnetic field \mathbf{B} inclined at a small angle, $\alpha \ll 1$ (in radians), to the target. The ordering $\alpha \gg \sqrt{Zm_e/m_i}$, where m_e and m_i are the electron and ion mass respectively, and Z is the charge state of the ion, is assumed such that electrons are adiabatic. The size of electrostatic potential variations near the wall is $\sim T_e/e$, where T_e is the electron temperature and e is the proton charge. A simple model, assuming a negligible electron gyroradius, is used to calculate the wall potential. The electric field \mathbf{E} near the wall accelerates ions, although a substantial fraction of the kinetic energy acquired by the ions goes in the components tangential to the target: parallel streaming and, mostly, $\mathbf{E} \times \mathbf{B}$ drift. The normal velocity of an ion at the target, v_x , is a combination of: the gyrophase dependent velocity of the ion due to the orbit moving a fraction α of a gyroradius closer to the target at each gyration, giving $v_x \sim \sqrt{\alpha} v_{t,i}$, where $v_{t,i} = \sqrt{2T_i/m_i}$ is the ion thermal velocity and T_i is the ion temperature; the velocity acquired from the electric force, which typically overcomes the magnetic force close to the target, giving $v_x \sim v_B = \sqrt{ZT_e/m_i}$, where v_B is the Bohm velocity. We derive expressions for the velocity distribution of ions at the target using a large gyro-orbit model, shown to be accurate for $\tau = T_i/(ZT_e) \gg 1$ and qualitatively correct for $\tau \sim 1$. Importantly, the model captures how the kinetic energy of an ion reaching the target is split between the normal and tangential velocity components, which is expected to inform sputtering predictions.

1. Introduction

When plasma is in contact with a solid surface — such as in fusion experiments (Stangeby 2000), Hall thrusters (Boeuf 2017), plasma probes (Hutchinson 2002), magnetic filters (Anders *et al.* 1995), and orbiting spacecraft (Hastings 1995) — the resulting interaction affects both the plasma and the surface. Among the many plasma-surface interaction processes, one that is of particular concern is sputtering, where an ion from the plasma reaches the surface material and knocks an atom off the surface. Ionization of sputtered atoms in the plasma produces impurities, thus altering the plasma. Moreover, in the long run sputtering causes erosion of the surface material. The amount of sputtering depends on a wide variety of factors, including surface material, surface roughness, plasma conditions and velocity distributions of particles striking the target (Krasheninnikov & Kukushkin 2017; Cohen & Ryutov 1998*b*; Drobný *et al.* 2017; Khaziev & Curreli 2015; Siddiqui *et al.* 2016; Lasa *et al.* 2020).

In this paper, we focus on the calculation of the distribution function of plasma ions

† Email address for correspondence: ale.gerald@gmail.com

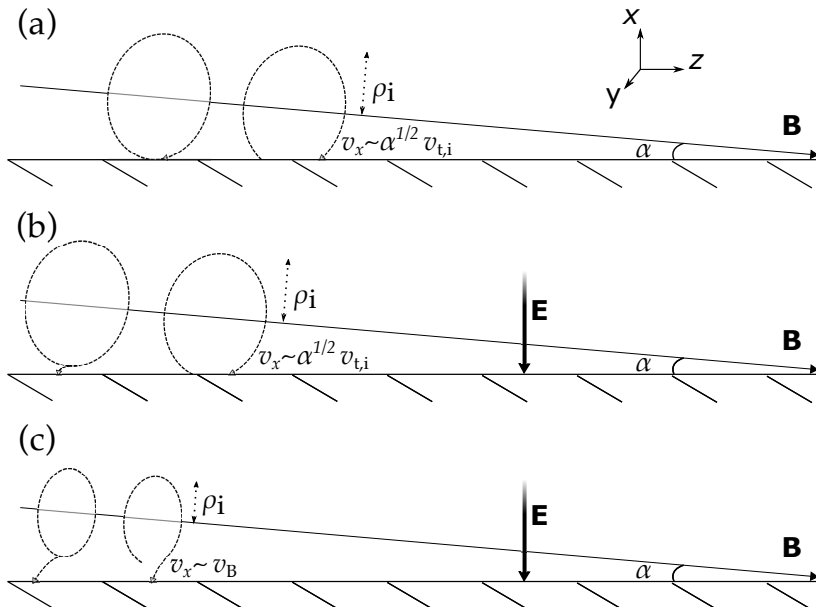


FIGURE 1. Cartoons of ion gyro-orbits, whose gyro-radii is ρ_i , reaching the target when the angle between the magnetic field \mathbf{B} and the target is small, $\alpha \ll 1$. The axes (x, y, z) are labelled. (a) With no normal electric field, the circular orbit moves closer to the target by $\alpha\rho_i$ after a gyroperiod and thus the normal velocity of an ion at the target is $v_x \sim \sqrt{\alpha}v_{t,i}$. (b,c) With the magnetic presheath and Debye sheath electric field \mathbf{E} , ions are accelerated to $v_x \sim \sqrt{\alpha v_{t,i}^2 + v_B^2}$.

striking the solid surface. We consider the target surface — or wall — to be smooth, planar and absorbing all incident particles. We consider a plasma magnetized by a uniform magnetic field \mathbf{B} , with one ion species. The angle between the magnetic field and the wall is taken to be small, $\alpha \ll 1$ (measured in radians unless otherwise indicated). This situation is particularly relevant in fusion plasmas, where divertors are designed so that the angle between incident magnetic field lines and the target surface is as small as possible. We define a set of right-handed cartesian axes (x, y, z) where x measures the distance from the wall, z measure displacements in the direction tangential to the wall, such that the magnetic field is in the x - z plane, and y measures displacements in the remaining direction. The axes are shown on the top-right of figure 1. For simplicity, we assume no gradients tangential to the wall: thus, the only gradients are in the x direction.

The standard picture of the plasma-wall boundary is as follows. Close to the wall, there is a thin positively charged layer called a Debye sheath, with a characteristic size of a few Debye lengths $\lambda_D = \sqrt{\epsilon_0 T_e / e^2 n_e}$, where a strong electric field $\mathbf{E} = -\nabla\phi$ directed towards the target is present to repel electrons (Riemann 1991; Hershkovitz 2005; Baalrud *et al.* 2019). Here, e is the proton charge, n_e is the number density of the electrons, ϵ_0 is the permittivity of free space, T_e is the temperature of the electrons, and $\phi(x)$ is the electrostatic potential as a function of the distance from the wall. The purpose of the electric field is to achieve a steady state with comparable (or, in ambipolar conditions, equal) fluxes of ions and electrons to the wall. The size of electrostatic potential variations necessary to repel electrons is $\phi \sim T_e/e$. The kinetic energy gained by an ion of charge Ze in such a potential is $Ze\phi \sim ZT_e$. Hence, the parameter

$$\tau = \frac{T_i}{ZT_e}, \quad (1.1)$$

where T_i is the ion temperature, determines the ratio of *ion thermal energy divided by ion kinetic energy gained from the electric field*. At the edge of a fusion device one often finds $\tau \gtrsim 1$ (Mosetto *et al.* 2015). Poisson's equation,

$$\varepsilon_0 \phi''(x) = Z n_i(x) - n_e(x), \quad (1.2)$$

relates the charge separation to the electrostatic potential in the Debye sheath, where $x \sim \lambda_D$. At distances from the wall comparable to the ion sound gyroradius, ρ_s , the ion population is depleted due to a combination of ion gyro-orbit losses and acceleration of ions by the electric field, as schematically shown in figure 1. Here, $\rho_s = c_s/\Omega$, where $c_s = \sqrt{(ZT_e + T_i)/m_i}$ is the ion sound speed, $\Omega = ZeB/m_i$ is the ion gyrofrequency, $B = |\mathbf{B}|$ and m_i is the ion mass. Since typically $\lambda_D \ll \rho_s$, the region $x \sim \rho_s$ can be assumed to be quasineutral,

$$Z n_i(x) \simeq n_e(x), \quad (1.3)$$

and is referred to as *magnetic presheath* (and sometimes as Chodura sheath). A substantial fraction of the electrostatic potential drop between the plasma and the wall must occur in the magnetic presheath, as an electric field is necessary to adjust the electron and ion densities such that (1.3) is preserved. At distances from the target assumed to be even larger, $d_c \gg \rho_s$, ions tend to collide with neutrals or other ions before reaching the target. Thus, the magnetic presheath and Debye sheath can be assumed to be collisionless. In this paper, the distribution function of ions is assumed known at distances from the target corresponding to $\rho_s \ll x \ll d_c$: where ions travelling towards the target have passed the collisional layer but have not reached the magnetic presheath.

An approach that describes all the phenomena at play close to the wall, including the effect of the collisional layer, is to numerically solve the kinetic Vlasov equation for the ions and electrons self-consistently with the Poisson equation for the electrostatic potential (Coulette & Manfredi 2016). An alternative, equally complete, approach is the particle-in-cell (PIC) method (Tskhakaya & Kuhn 2003; Khaziev & Curreli 2015). Both the Vlasov and the PIC approaches offer the most complete description of the plasma, but can be computationally expensive. Simplifying models can offer more immediate calculations. For example, taking into account gyro-orbit losses at the wall, but ignoring the electric field, one can solve for distribution functions at the wall analytically, assuming an incoming Maxwellian (Parks & Lippmann 1994) or more refined boundary conditions (Gunn *et al.* 2017). For grazing angles, this model is accurate for $\tau \gg 1/\alpha$ (Geraldini *et al.* 2019). However, in neglecting the electric field it assumes that some ions can reach the target travelling tangentially, as shown in figure 1(a)†. By introducing an ad hoc analytical electrostatic potential function close to the wall to model the effect of gyro-orbit distortion, Borodkina *et al.* (2016) numerically solved for ion trajectories near the target, finding a substantial effect on erosion coefficients, as was also suggested by Siddiqui *et al.* (2016). In Geraldini *et al.* (2018, 2019), the ion trajectories in the magnetic presheath were solved using an asymptotic expansion in $\alpha \ll 1$ (Cohen & Ryutov 1998*a*), with a numerical scheme to efficiently calculate the self-consistent electrostatic potential. Velocity distributions of ions reaching the Debye sheath, consistent with a quasineutral magnetic presheath, were thus obtained. While this model applies only to grazing angles, it provides an efficient way to solve self-consistently for the effect of the electric field on ion trajectories in the magnetic presheath.

† This issue can be seemingly resolved by adding the kinetic energy gain of an ion in the Debye sheath ad hoc, although the velocity distributions thus obtained vastly overestimate the energy going into the normal component of the ion velocity and thus overestimate the angle of impact of ions with the target.

In this paper, a simple electron model, assuming a small electron gyroradius such that $\rho_e \ll \lambda_D$, is used to obtain the wall potential, and thus the Debye sheath potential drop. This is used to obtain the ion distribution function at the target from the ion distribution function reaching the Debye sheath. Ion distribution functions reaching the Debye sheath are obtained in two different ways:

- (i) using the full numerical solution of the asymptotic theory (Geraldini *et al.* 2018);
- (ii) using a large gyro-orbit model.

Much of the paper is devoted to the derivation of the large gyro-orbit model (ii) and to the justification of its quantitative accuracy for $\tau \gg 1$. Numerical results using methods (i)-(ii) indicate that the large gyro-orbit model adequately captures the wall-normal velocity distribution at the Debye sheath entrance and the ion energy-angle distributions at the target for $\alpha \leq 5^\circ$ and $\tau \gtrsim 1$, subject to the validity of the adiabatic electron approximation $\alpha \gg \sqrt{Zm_e/m_i}$. A simple, albeit crude, reduction of the large gyro-orbit model is suggested in order to calculate ion distribution functions for $\alpha \sim \sqrt{Zm_e/m_i}$ and $\rho_e \ll \lambda_D$, although its accuracy will have to be further tested. Like in Geraldini *et al.* (2018, 2019), we assume a functional form for the incoming distribution function at $\rho_s \ll x \ll d_c$ that is parameterised by τ .

The rest of the paper is structured as follows. In section 2, the orderings assumed in this work are presented and discussed. In section 3, the electron current reaching the wall is related to the wall potential, and the Boltzmann distribution for the electron density is derived for $\alpha \gg \sqrt{Zm_e/m_i}$. In section 4 ion trajectories in the collisionless magnetic presheath and Debye sheath regions are analyzed. The velocity distributions of ions reaching the Debye sheath and of ions striking the target are obtained in section 5 using the characteristics of the ion motion. The trajectories of ions in large gyro-orbits are analyzed in section 6, and a closed set of analytical expressions for the velocity distribution of large gyro-orbits reaching the Debye sheath and striking the target is obtained. In section 7 distribution functions obtained using the asymptotic numerical solutions (i) are compared with the large gyro-orbit model (ii), with good agreement. Finally, in section 8, the results of the paper are summarized.

2. Orderings

This section introduces and summarizes the orderings assumed in this work.

With the electrostatic potential ordered as $\phi \sim T_e/e$, the kinetic energy gained by an ion of charge Ze in such a potential is $Ze\phi \sim ZT_e$. Hence, the characteristic speed of an ion due to the energy gained from the electric field is the Bohm velocity $v_B = \sqrt{ZT_e/m_i}$. The thermal speed of an ion is $v_{t,i} = \sqrt{2T_i/m_i}$. The ion velocity, denoted $\mathbf{v} = (v_x, v_y, v_z)$ where v_i is the velocity component in the i th direction, is therefore ordered such that $|\mathbf{v}| \sim c_s$. The depletion of ion gyro-orbits modifies the estimate for v_x , as the component of the gyration velocity in the x direction for an ion reaching the wall is suppressed to $v_x \sim \sqrt{\alpha}v_{t,i}$ by gyro-orbit losses. This estimate can be obtained as follows. Consider the circular ion gyro-orbit, with no electric field, shown in figure 1(a). The component of the velocity parallel to the magnetic field is denoted v_{\parallel} and the magnitude of the gyrating component of the velocity is denoted v_{\perp} . The gyrophase angle of the ion is denoted φ . In the small-angle approximation, $\sin \alpha \simeq \alpha$, $\cos \alpha \simeq 1$, and the component of the velocity normal to the wall is given by $v_x \simeq v_{\perp} \sin \varphi - \alpha v_{\parallel}$. If the gyro-orbit touches the wall approximately tangentially at a time $t = 0$, the distance from the wall at a later time t is $x \simeq (v_{\perp}/\Omega)(1 - \cos \varphi) - \alpha v_{\parallel}t$. After a full gyro-period $2\pi/\Omega$, the orbit has drifted a little closer to the wall and so the gyrophase angle corresponding to $x = 0$ is no longer

$\varphi = 0$, yet has only changed by a small amount. Solving for $x = 0$ at $t = 2\pi/\Omega$ with $1 - \cos \varphi \simeq \varphi^2/2$ gives $\varphi \simeq \sqrt{4\pi\alpha v_{\parallel}/v_{\perp}}$, and thus $v_x \simeq -\sqrt{4\pi\alpha v_{\parallel}v_{\perp}}$ (Cohen & Ryutov 1998a). The piece of v_x equal to $-\alpha v_{\parallel}$ is smaller by a factor of $\sqrt{\alpha v_{\parallel}/(4\pi v_{\perp})}$. Since by ignoring the electric field we expect $v_{\parallel} \sim v_{\perp} \sim v_{t,i}$, the estimate $v_x \sim \sqrt{\alpha} v_{t,i}$ follows. The electric field, however, can still accelerate ions to $v_x \sim v_B$, as depicted schematically in figure 1(b-c). Combining these estimates, the velocity of the ion at the target satisfies $v_x \sim v_B \sqrt{1 + \alpha\tau}$ and $v_y \sim v_z \sim c_s$.

As was discussed in the introduction, the Debye sheath, the magnetic presheath and the collisional region are assumed to satisfy the scale separation $\lambda_D \ll \rho_s \ll d_c$. Since at distances $x \sim d_c \gg \rho_s$ the ion motion is restricted along a field line, the size of the collisional region can be expressed as $d_c \sim \alpha \lambda_{\text{mfp}}$, where λ_{mfp} is the mean free path of an ion near the target. Therefore, the angle α must satisfy $\alpha \gg \rho_s/\lambda_{\text{mfp}}$ in order for $\rho_s \ll d_c$ to be valid.

In order to simplify the treatment of the electrons, the electron gyroradius ρ_e is assumed much smaller than the Debye length, such that $\rho_e \ll \lambda_D$ (Stangeby 2012; Loizu *et al.* 2012). Being tightly bound to the magnetic field lines, electrons have to travel along the magnetic field at $\sim v_{t,e}$ in order to reach the wall. Conversely, the typical ion velocity close to the wall is $\sim v_B \sqrt{1 + \alpha\tau}$ towards the wall. The self-consistent wall potential repels most of the electrons from the Debye sheath only provided they reach the wall significantly more quickly than the ions, such that $\alpha v_{t,e} \gg v_B \sqrt{1 + \alpha\tau}$, giving rise to the ordering $\sqrt{(1 + \alpha\tau)Zm_e/m_i} \ll \alpha$. For $\alpha\tau \gg 1$, this gives $\alpha \gg m_e\tau Z/m_i$; in order for both orderings to be simultaneously satisfied we require $1/\alpha \ll \tau \ll \alpha m_i/m_e Z$, giving $\alpha \gg \sqrt{Zm_e/m_i}$, which is equivalent to the ordering obtained for $\alpha\tau \lesssim 1$. With this ordering, most electrons are repelled from the wall in the Debye sheath and so the electrons can be assumed to be adiabatic across the whole magnetic presheath.

To summarize, the physical length scales are ordered according to

$$\rho_e \ll \lambda_D \ll \rho_s \ll d_c, \quad (2.1)$$

while the angle and mass ratio are assumed to satisfy

$$\sqrt{\frac{Zm_e}{m_i}} \ll \alpha \ll 1. \quad (2.2)$$

The validity of these orderings is examined for a current fusion experiment such as JET. In a Deuterium plasma, the angle obtained from the square root of mass ratio is $\sqrt{m_e/m_i} \approx 0.02 \text{ rad} \sim 1^\circ$. From Militello & Fundamenski (2011), we estimate for JET: $B \sim 2 \text{ T}$, $T_e \sim T_i \sim 50 \text{ eV}$, $n_e \sim n_i \sim 10^{19} \text{ m}^{-3}$, giving $\rho_s \sim 1 \text{ mm}$, $\lambda_D \sim \rho_e \sim 0.02 \text{ mm}$ and $\alpha \approx 0.07 \text{ rad} \approx 4^\circ$. Since the orderings $\sqrt{m_e/m_i} \ll \alpha$ and $\rho_e \ll \lambda_D$ seem to not be well-satisfied in fusion devices, it will be necessary to study in more detail the effect of electron inertia and gyroradius.

3. Electron model

In this section, Maxwellian electrons are assumed to enter the magnetic presheath, and the relationship between the electron current to the wall and the electrostatic potential at the wall is obtained. An approximate expression, valid in the ordering (2.2), for the electron density in the magnetic presheath is also obtained.

According to (2.1), the electron gyroradius is so small that electrons are essentially tied to the magnetic field line, as shown in figure 2. The electrons stream parallel to the magnetic field with a velocity given by w_{\parallel} , while their gyro-motion at $\rho_e \ll \lambda_D$ is

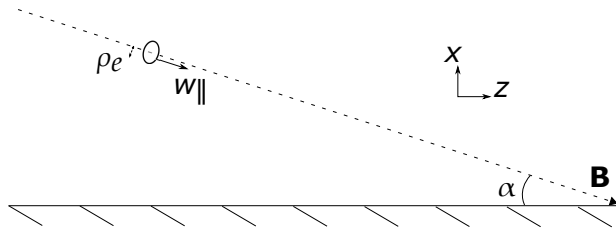


FIGURE 2. Cartoon of an electron gyro-orbit, whose gyro-radius is ρ_e , streaming towards the wall along the magnetic field \mathbf{B} with velocity w_{\parallel} .

unaffected. The electron distribution function *entering* (that is, for $w_{\parallel} > 0$) the magnetic presheath is assumed a half-Maxwellian,

$$g_{\text{MPE}}(w_{\parallel}) = Z\bar{n}_{\text{MPE}} \left(\frac{m_e}{2\pi T_e} \right)^{3/2} \exp\left(-\frac{m_e w_{\parallel}^2}{2T_e}\right) \text{ for } w_{\parallel} > 0, \quad (3.1)$$

with density denoted as Zn_{MPE} ,

$$Zn_{\text{MPE}} = \int_{-\infty}^{\infty} g_{\text{MPE}}(w_{\parallel}) dw_{\parallel}. \quad (3.2)$$

Since the number of electrons that enter the presheath and come back out of it depends on the potential at the wall, denoted $\phi_{\text{W}} = \phi(0)$, \bar{n}_{MPE} depends on n_{MPE} and ϕ_{W} .

In the magnetic presheath and Debye sheath, the component of the electron velocity parallel to the magnetic field as a function of x is obtained by energy conservation

$$w_{\parallel} = \sigma \sqrt{w_{\parallel\text{MPE}}^2 + \frac{2e\phi(x)}{m_e}}, \quad (3.3)$$

where $w_{\parallel\text{MPE}}$ is the electron velocity at the magnetic presheath entrance. The $\mathbf{E} \times \mathbf{B}$ and gyration velocities of an electron remain unaffected by electrostatic potential variations, as these occur over length scales much larger than the electron gyroradius, $\lambda_{\text{D}} \gg \rho_e$. In (3.3), $\sigma = \pm 1$ for those electrons reflected before reaching the wall and $\sigma = 1$ for those electrons that are not reflected. At $x = 0$ the electron velocity is zero if $w_{\parallel\text{MPE}}^2 = -2e\phi_{\text{W}}/m_e$. Hence, reflected electrons satisfy

$$w_{\parallel\text{MPE}}^2 < -\frac{2e\phi_{\text{W}}}{m_e}, \quad (3.4)$$

as they cannot reach $x = 0$. The full electron distribution function at the magnetic presheath entrance is thus

$$g_{\text{MPE}}(w_{\parallel}) = Z\bar{n}_{\text{MPE}} \left(\frac{m_e}{2\pi T_e} \right)^{1/2} \exp\left(-\frac{m_e w_{\parallel}^2}{2T_e}\right) \Theta\left(w_{\parallel} + \sqrt{-\frac{2e\phi_{\text{W}}}{m_e}}\right). \quad (3.5)$$

where Θ is the Heaviside step function,

$$\Theta(\xi) = \begin{cases} 1 & \text{for } \xi \geq 0 \\ 0 & \text{for } \xi < 0. \end{cases} \quad (3.6)$$

Assuming $\text{erf}(\sqrt{-e\phi_{\text{W}}/T_e}) \simeq 1$, which will be justified in the next paragraph, we obtain

$$\bar{n}_{\text{MPE}} = \frac{2n_{\text{MPE}}}{\left(1 + \text{erf}\left(\sqrt{-e\phi_{\text{W}}/T_e}\right)\right)} \simeq n_{\text{MPE}}. \quad (3.7)$$

From the electron velocity distribution in (3.5) the electron current $j_{e\parallel}$ is obtained from the first moment of the distribution function (the flux of electrons) multiplied by the electron charge, $-e$. The electron current directed towards the wall is the geometric projection of the parallel current, $j_{e,x} = -j_{e\parallel} \sin \alpha \simeq -\alpha j_{e\parallel}$,

$$j_{e,x} \simeq -\alpha Z n_{\text{MPE}} \left(\frac{T_e}{2\pi m_e} \right)^{1/2} \exp\left(\frac{e\phi_{\text{W}}}{T_e}\right). \quad (3.8)$$

The electron and ion current are assumed to be similar in size, and the size of the ion current at the magnetic presheath entrance is assumed to be of the order of the sound speed — as expected from the Bohm-Chodura condition (Chodura 1982; Geraldini *et al.* 2018) — giving $j_{e,x} \sim -\alpha Z n_{\text{MPE}} c_s$. Hence, the electrostatic potential at the wall is

$$\frac{e\phi_{\text{W}}}{T_e} \sim \ln \left(\sqrt{\frac{2\pi m_e (1 + \tau)}{m_i}} \right) \quad (3.9)$$

where $\sqrt{2\pi m_e (1 + \tau)/m_i} \ll 1$, justifying $\text{erf}(\sqrt{-e\phi_{\text{W}}/T_e}) \simeq 1$. The electron distribution function at any point in the magnetic presheath and Debye sheath is

$$g(x, w_{\parallel}) \simeq Z n_{\text{MPE}} \left(\frac{m_e}{2\pi T_e} \right)^{1/2} \exp\left(\frac{e\phi(x)}{T_e} - \frac{m_e w_{\parallel}^2}{2T_e}\right) \Theta \left(\sqrt{\frac{2e(\phi(x) - \phi_{\text{W}})}{m_e}} - w_{\parallel} \right). \quad (3.10)$$

Hence, the electron density is

$$n_e(x) \simeq \frac{1}{2} \left(1 + \text{erf} \left(\sqrt{\frac{e(\phi(x) - \phi_{\text{W}})}{T_e}} \right) \right) Z n_{\text{MPE}} \exp\left(\frac{e\phi(x)}{T_e}\right). \quad (3.11)$$

In the magnetic presheath the electrostatic potential is at its smallest in the region $\lambda_{\text{D}} \ll x \ll \rho_s$, known as the Debye sheath entrance, where $\phi(x) \simeq \phi_{\text{DSE}}$. Thus, provided $\text{erf}(\sqrt{e(\phi_{\text{DSE}} - \phi_{\text{W}})/T_e}) \simeq 1$, the electron density in the magnetic presheath is given by the Boltzmann distribution

$$n_e(x) \simeq Z n_{\text{MPE}} \exp\left(\frac{e\phi(x)}{T_e}\right). \quad (3.12)$$

The ion density at the Debye sheath entrance is ordered as follows. The ion flow speed parallel to the magnetic field at the magnetic presheath entrance, $\rho_s \ll x \ll d_c$, is of the order of the sound speed $\sim c_s$. Thus, the mean flow velocity of ions towards the target is $\alpha c_s \sim \alpha \sqrt{1 + \tau} v_{\text{B}}$. At the Debye sheath entrance, the size of the flow velocity is given by $v_x \sim \sqrt{1 + \alpha \tau} v_{\text{B}}$. Thus, due to steady-state ion conservation, the ion density at the Debye sheath entrance is $\sim \alpha n_{\text{MPE}} \sqrt{1 + \tau} / \sqrt{1 + \alpha \tau}$. Hence,

$$\frac{e\phi_{\text{DSE}}}{T_e} \sim \ln \left(\frac{\alpha \sqrt{1 + \tau}}{\sqrt{1 + \alpha \tau}} \right) \quad (3.13)$$

and

$$\frac{e(\phi_{\text{DSE}} - \phi_{\text{W}})}{T_e} \sim \ln \left(\frac{1}{\alpha} \sqrt{\frac{2\pi m_e (1 + \alpha \tau)}{m_i}} \right). \quad (3.14)$$

From equation (3.14) and the ordering $\sqrt{Zm_e/m_i} \ll \alpha$, equation (3.12) for the electron density in the magnetic presheath is justified.

The results of this section that will be used in the rest of the paper are equation (3.12) for the electron density in the magnetic presheath, and equation (3.8) for the relationship between electron current and wall potential.

4. Ion trajectories

In this section the trajectories of ions in the magnetic presheath and the Debye sheath are analyzed in detail. The goal of this section is to relate the velocity of an ion at the Debye sheath entrance, and at the target, to the energy and magnetic moment of its circular gyro-orbit at the magnetic presheath entrance $\rho_s \ll x \ll d_c$.

The equations of motion of ions in the magnetic presheath, under the influence of a wall-normal electrostatic electric field and a magnetic field at an angle α with the wall, are

$$\dot{v}_x = -\frac{\Omega\phi'(x)}{B} + \Omega v_y \cos \alpha, \quad (4.1)$$

$$\dot{v}_y = -\Omega v_x \cos \alpha - \Omega v_z \sin \alpha, \quad (4.2)$$

$$\dot{v}_z = \Omega v_y \sin \alpha. \quad (4.3)$$

For *grazing* angles, $\alpha \ll 1$, the equations simplify to

$$\dot{v}_x \simeq -\frac{\Omega\phi'(x)}{B} + \Omega v_y, \quad (4.4)$$

$$\dot{v}_y \simeq -\Omega v_x - \alpha\Omega v_z + O(\alpha^2\Omega v_{t,i}), \quad (4.5)$$

$$\dot{v}_z \simeq \alpha\Omega v_y + O(\alpha^3\Omega v_{t,i}). \quad (4.6)$$

It will be useful to introduce two *orbit parameters*,

$$\bar{x} = x + \frac{v_y}{\Omega}, \quad (4.7)$$

$$U_\perp = \frac{1}{2}v_x^2 + \frac{1}{2}v_y^2 + \frac{\Omega\phi(x)}{B}, \quad (4.8)$$

whose time derivatives satisfy $\dot{\bar{x}} = -\alpha v_z + O(\alpha^2 v_{t,i})$ and $\dot{U}_\perp = -\alpha\Omega v_y v_z + O(\alpha^2\Omega v_{t,i}^2)$. The third orbit parameter,

$$U = \frac{1}{2}v_x^2 + \frac{1}{2}v_x^2 + \frac{1}{2}v_x^2 + \frac{\Omega\phi(x)}{B}, \quad (4.9)$$

is just the total energy of an ion and is exactly conserved. From the definitions (4.7)-(4.8), we obtain

$$v_z = \sqrt{2(U - U_\perp)}, \quad (4.10)$$

$$v_y = -\Omega(x - \bar{x}), \quad (4.11)$$

and

$$v_x = \pm\sqrt{2(U_\perp - \chi(x, \bar{x}))}, \quad (4.12)$$

where in (4.12) an effective potential function,

$$\chi(x; \bar{x}) = \frac{1}{2} \Omega^2 (x - \bar{x})^2 + \frac{\Omega \phi(x)}{B}, \quad (4.13)$$

was introduced. Note that, to lowest order in $\alpha \ll 1$, v_z is equivalent to the velocity component parallel to the magnetic field. The electric field slowly (due to the grazing angle) pushes ions in the direction parallel to the magnetic field towards larger v_z (Geraldini *et al.* 2017). Since all ions entering the magnetic presheath have $v_z \geq 0$, and v_z increases in the magnetic presheath, in (4.10) we set $v_z \geq 0$.

The orbit parameter \bar{x} is referred to as the *orbit position*, and U_\perp as the *perpendicular energy* (perpendicular to the magnetic field). Since $\dot{\bar{x}}/v_{t,i} \sim \dot{U}_\perp/v_{t,i}^2 \sim \alpha \Omega \ll \dot{v}_x/v_{t,i} \sim \Omega$, the orbit position and perpendicular energy only change by a very small amount during a time $\sim 1/\Omega$. Neglecting the small change in the orbit parameters (which is a good approximation for a time $\ll 1/(\alpha \Omega)$), particle orbits are solved for as follows. Consider a local minimum of the effective potential, $\chi_m(\bar{x}) = \chi(x_m, \bar{x})$, such that

$$\chi'(x_m, \bar{x}) = \Omega^2(x_m - \bar{x}) + \frac{\Omega \phi'(x_m)}{B} = 0, \quad (4.14)$$

and

$$\chi''(x_m) = \Omega^2 + \frac{\Omega \phi''(x_m)}{B} > 0. \quad (4.15)$$

In the neighbourhood of this minimum, the motion is periodic with turning points $x_b < x_m$ (for bottom) and $x_t > x_m$ (for “top”) obtained by solving for where the ion is stationary, $v_x = 0$, giving $U_\perp = \chi(x_{b,t}, \bar{x})$. Note that, although not made explicit, the quantities x_M , x_b and x_t are functions of U_\perp and \bar{x} .

Though \bar{x} and U_\perp change by a small amount during one period of the approximately closed orbit, the cumulative effect of these small changes is important after a number of periods which is large, $\sim 1/\alpha$. Nonetheless, the quasi-periodic motion of the ion has an adiabatic invariant

$$\mu = \frac{1}{\pi} \int_{x_b}^{x_t} \sqrt{2(U_\perp - \chi(x, \bar{x}))} dx, \quad (4.16)$$

which is conserved to lowest order in $\alpha \ll 1$ during the entire ion trajectory in the magnetic presheath (Cohen & Ryutov 1998a).

Approximately periodic motion only occurs insofar as it is not interrupted by the absorbing wall. However, if the ion motion is periodic to lowest order in α , then no ion trajectory at this level of accuracy describes an ion reaching the wall. It is clear that the small variations in \bar{x} and U_\perp occurring over a short timescale must be retained to find the trajectory of those ions that are about to reach the wall. If the perpendicular energy becomes larger than a threshold value, the ion gyro-orbit becomes sufficiently large that the bottom bounce point disappears. The threshold value of U_\perp is the maximum value of the effective potential function between the position of the minimum, $x = x_m$, and the wall, $x = 0$,

$$\chi_M(\bar{x}) \equiv \chi(x_M; \bar{x}) = \max_{x \in [0, x_m]} \chi(x, \bar{x}). \quad (4.17)$$

As will be shown in section 6.1, with adiabatic electrons the position x_M is always a stationary point in the magnetic presheath. Since the variation of U_\perp and \bar{x} is slow compared to the timescale of ion motion, ions quickly reach the wall once $U_\perp > \chi_M(\bar{x})$, and therefore these ions have $U_\perp \simeq \chi_M(\bar{x})$. Any ion reaching the wall must — since it

comes from an approximately periodic orbit — have a value of orbit position such that an effective potential minimum exists. From equation (4.14), the smallest value of orbit position, denoted \bar{x}_c , for which an ion can reach the wall is given by

$$\bar{x}_c = \min \left(x + \frac{\phi'(x)}{\Omega B} \right). \quad (4.18)$$

Note that as the wall is approached x decreases while the electric field $\phi'(x)$ increases. If the increase in $\phi'(x)$ is not large enough, $\bar{x}_c = \phi'(0)/\Omega B$ is obtained. With adiabatic electrons, however, the increase of $\phi'(x)$ as the wall is approached is always large enough to give $\bar{x}_c = x_c + \phi'(x_c)/(\Omega B)$ where $x_c \neq 0$ is the position of the minimum of the function on the right hand side of (4.18).

For ions at the wall or in the Debye sheath, $x \sim \lambda_D \ll \rho_s$, the orbit position \bar{x} and the tangential component v_y of the velocity are equivalent to within a constant factor of Ω : from equation (4.11), $v_y = \Omega \bar{x} (1 + O(\lambda_D/\rho_s))$ for $x \sim \lambda_D$, giving

$$v_y \simeq \Omega \bar{x}. \quad (4.19)$$

For every ion in the Debye sheath, we can trace back its trajectory to a quasiperiodic orbit. The associated value of μ is a function of \bar{x} ($\simeq v_y/\Omega$) only, since $U_\perp \simeq \chi_M(\bar{x})$ for ions reaching the target,

$$\mu_{\text{op}}(\bar{x}) = \frac{1}{\pi} \int_{x_M}^{x_{t,M}} \sqrt{2(\chi_M(\bar{x}) - \chi(x, \bar{x}))} dx. \quad (4.20)$$

The value of v_z is determined by the total energy U ,

$$v_z \simeq \sqrt{2(U - \chi_M(\bar{x}))}. \quad (4.21)$$

The value of v_x is related to the value of \bar{x} , and thus to the value of the adiabatic invariant μ , by $v_x \simeq \sqrt{2(\chi_M(\bar{x}) - \chi(x, \bar{x}))}$. However, there is a small range of allowed values of v_x due to the small displacement of the ion gyro-orbit by $\alpha \rho_i$ closer to the wall during the last ion gyro-orbit (see figure 1). Although small, the size of this range determines the number of ions reaching the wall for any value of \bar{x} and U , and therefore it must be quantified in order to accurately determine the density and distribution function of ions reaching the target (Geraldini *et al.* 2018).

The transition from a quasiperiodic orbit, with at least one turning point in its future trajectory, to an open orbit, with no turning points in its future trajectory, occurs as follows. The small change of \bar{x} and U_\perp causes the value of $U_\perp - \chi_M(\bar{x})$ to increase until $U_\perp > \chi_M(\bar{x})$. The increase is slow, $d(U_\perp - \chi_M(\bar{x}))/dt \sim \alpha v_{t,i}^2$, and thus the change in $U_\perp - \chi_M(\bar{x})$ incurred by an ion transitioning from $U_\perp < \chi_M(\bar{x})$ to $U_\perp > \chi_M(\bar{x})$ can be calculated approximately by assuming a periodic orbit with fixed $U_\perp = \chi_M(\bar{x})$, as shown in Appendix A. Such an orbit is fictitious: it has a bottom turning point coinciding with the position of the effective potential maximum, x_M , and takes an infinite time† to reach x_M and also to turn around and leave x_M . The true orbit turns at $x_b > x_M$ (with $U_\perp < \chi_M$), then once more at x_t , and then passes x_M (with $U_\perp > \chi_M$) in a finite time $\sim \ln(1/\alpha)/\Omega$ moving towards the wall, as shown in Appendix A. Yet, despite the approximate orbit being qualitatively different from the true orbit, the change in $U_\perp - \chi_M(\bar{x})$ is accurate to lowest order in α when calculated from the approximate orbit because the long time spent near x_M does not contribute to a significant change in $U_\perp - \chi_M(\bar{x})$; the time derivatives of U_\perp and of $\chi_M(\bar{x})$ coincide at $x = x_M$. The overall

† For those electrostatic potential profiles that result in $x_M \neq 0$, consistent with adiabatic electrons.

change in the quantity $U_{\perp} - \chi_M(\bar{x})$ during the last gyro-orbit is

$$\Delta_M(\bar{x}, U) = 2\pi\alpha\Omega^2 V_{\parallel}(\chi_M(\bar{x}), U) \frac{d\mu_{\text{op}}(\bar{x})}{d\bar{x}}, \quad (4.22)$$

as shown in Appendix A. Therefore, for a given value of \bar{x} (or μ) and U , the possible values of v_x are

$$\chi_M(\bar{x}) - \frac{1}{2}\Omega\bar{x}^2 - \frac{\Omega\phi(x)}{B} \leq \frac{v_x^2}{2} < \chi_M(\bar{x}) + \Delta_M(\bar{x}, U) - \frac{1}{2}\Omega\bar{x}^2 - \frac{\Omega\phi(x)}{B}. \quad (4.23)$$

Equation (4.23) is valid at any point in the Debye sheath, *including the Debye sheath entrance and the wall*. For $\sqrt{Zm_e/m_i} \ll 1$ the Debye sheath repels most electrons from the wall and attracts all ions to the wall, so ions in the Debye sheath must satisfy $v_x < 0$.

5. Ion velocity distribution

The ion distribution function at the magnetic presheath entrance, $\rho_s \ll x \ll d_c$ is denoted $f_{\text{MPE}}(v_x, v_y, v_z)$. The exact distribution function in this region includes a small number of ions with $v_z < 0$, that are travelling out of the magnetic presheath towards the collisional presheath. However, to lowest order in $\rho_s \ll d_c$ the appropriate boundary condition is

$$f_{\text{MPE}}(v_z \leq 0) = 0, \quad (5.1)$$

such that there are no ions leaving the magnetic presheath back into the collisional presheath. At the magnetic presheath entrance, $\phi(x) = 0$ and so the adiabatic invariant is, from (4.16),

$$\mu = \frac{v_x^2 + v_y^2}{2\Omega}. \quad (5.2)$$

Equation (5.2) is equivalent to the magnetic moment to lowest order in $\alpha \ll 1$; the small difference is geometric and arises because v_x is not exactly perpendicular to the magnetic field. It can be shown that the distribution function is independent of the gyrophase angle (Cohen & Ryutov 1998*a*; Geraldini *et al.* 2017) and therefore can be expressed in the form $F(\mu, U)$. The relationship between f_{MPE} and F is

$$f_{\text{MPE}}(v_x, v_y, v_z) = F\left(\frac{v_x^2 + v_y^2}{2\Omega}, \frac{v_x^2 + v_y^2 + v_z^2}{2}\right). \quad (5.3)$$

The function $F(\mu, U)$ is conserved across the magnetic presheath to lowest order in $\alpha \ll 1$, since μ and U are conserved.

The ion density at the magnetic presheath entrance, denoted n_{MPE} , is

$$n_{\text{MPE}} = 2\pi \int_0^{\infty} \Omega d\mu \int_{\Omega\mu}^{\infty} \frac{F(\mu, U) dU}{\sqrt{2(U - \Omega\mu)}} = \int f_{\text{MPE}}(v_x, v_y, v_z) d^3v. \quad (5.4)$$

The ion current towards the wall, $j_{i,x}$, is obtained by calculating the flow in the z direction, which approximately coincides with the direction parallel to the magnetic field, and multiplying by the geometric component, $-\alpha$, projecting this flow into the direction normal to the wall,

$$\frac{j_{i,x}}{Ze} \simeq -2\pi\alpha \int_0^{\infty} \Omega d\mu \int_{\Omega\mu}^{\infty} F(\mu, U) dU = -\alpha \int f_{\text{MPE}}(v_x, v_y, v_z) v_z d^3v. \quad (5.5)$$

We define the total current normal to the wall as

$$j_x = j_{e,x} + j_{i,x}. \quad (5.6)$$

From equations (3.8) and (5.6), the electrostatic potential at the wall is

$$\exp\left(\frac{e\phi_W}{T_e}\right) \simeq \frac{j_{i,x} - j_x}{\alpha Z e n_{\text{MPE}}} \left(\frac{2\pi m_e}{T_e}\right)^{1/2}. \quad (5.7)$$

with the ion current determined by (5.5), giving

$$\frac{e\phi_W}{T_e} \simeq \ln \left[\sqrt{\frac{2\pi m_e}{T_e}} \left(2\pi \int_0^\infty \Omega d\mu \int_{\Omega\mu}^\infty dUF(\mu, U) - \frac{j_x}{\alpha e n_{\text{MPE}}} \right) \right]. \quad (5.8)$$

The numerical results of this paper, presented in section 7, are obtained assuming ambipolarity, $j_x = 0$.

As was shown in section 4, every value of μ and U , originally associated with a circular gyro-orbit entering the magnetic presheath, is associated with a specific value of v_y and v_z and with a range of possible values of v_x entering the Debye sheath. At the Debye sheath entrance, the ion velocity is given by equation (4.23) with $\phi(x) = \phi_{\text{DSE}}$. Conservation of the phase space distribution function $F(\mu, U)$ leads to the following velocity distribution (Geraldini *et al.* 2018),

$$f_{\text{DSE}}(v_x, v_y, v_z) \simeq F(\mu_{\text{op}}(\bar{x}), U) \Theta(\bar{x} - \bar{x}_c) \Theta(-v_x) \\ \times \hat{\Pi} \left(\frac{1}{2} v_x^2 - \chi_{\text{M}}(\bar{x}) + \frac{1}{2} \Omega^2 \bar{x}^2 + \frac{\Omega \phi_{\text{DSE}}}{B}, 0, \Delta_{\text{M}}(\bar{x}, U) \right) \quad (5.9)$$

In Appendix B it is shown that the ion current normal to the wall calculated from (5.9) is equal to (5.5), and thus (5.9) satisfies ion conservation. At the wall, where $x = 0$, the range of possible values of v_x associated with each value of \bar{x} and U is given by equation (4.23) with $\phi(0) = \phi_W$,

$$f_{\text{W}}(v_x, v_y, v_z) \simeq F(\mu_{\text{op}}(\bar{x}), U) \Theta(\bar{x} - \bar{x}_c) \Theta(-v_x) \\ \times \hat{\Pi} \left(\frac{1}{2} v_x^2 - \chi_{\text{M}}(\bar{x}) + \frac{1}{2} \Omega^2 \bar{x}^2 + \frac{\Omega \phi_{\text{W}}}{B}, 0, \Delta_{\text{M}}(\bar{x}, U) \right). \quad (5.10)$$

In order to obtain f_{DSE} , and consequently f_{W} , it is necessary to determine the constants \bar{x}_c and ϕ_{DSE} , and the functions $\chi_{\text{M}}(\bar{x})$ and $\mu_{\text{op}}(\bar{x})$ (which, by equation (4.22), also determines $\Delta_{\text{M}}(\bar{x}, U)$). These quantities are specified by the electrostatic potential profile $\phi(x)$, which is obtained by solving the quasineutrality equation (1.3). Thus, equation (5.9) does not — *per se* — fully specify $f_{\text{DSE}}(v_x, v_y, v_z)$. In Geraldini *et al.* (2018) an expression for the ion density $n_i(x)$ for $\alpha \ll 1$, as a functional of the electrostatic potential $\phi(x)$, was derived. Using this expression, an iterative scheme to obtain the numerical solution $\phi(x)$ of the quasineutrality equation (1.3) was presented. In the next section, a closed set of equations for $f_{\text{DSE}}(v_x, v_y, v_z)$ is presented, which allows to bypass obtaining a numerical solution of $\phi(x)$ across the whole magnetic presheath, albeit with a loss of accuracy.

6. Large ion gyro-orbit model

In this section a model for f_{DSE} and f_{W} is obtained by deriving a closed set of equations for \bar{x}_c , ϕ_{DSE} , $\chi_{\text{M}}(\bar{x})$ and $\mu_{\text{op}}(\bar{x})$, which exploit the approximately undistorted nature of ion gyro-orbits in the limit $\tau \gg 1$. In section 6.1, the quasineutrality equation is expanded in the magnetic presheath close to the Debye sheath entrance, $\lambda_{\text{D}} \ll x \ll \rho_s$,

to obtain the relationship between the distribution function and electric field at the Debye sheath entrance. Then, in section 6.2 the expression for the electric field is used to derive expressions for the functions $\chi_M(\bar{x})$ and $\mu_{\text{op}}(\bar{x})$ that include the correction from the electric field acceleration near the wall. This procedure is strictly not self-consistent, as the expression for the electric field derived in the previous subsection is valid closer to the wall than where it is used. To determine the large orbit distribution function, only two parameters \bar{x}_c and ϕ_{DSE} remain to be specified. In section 6.3, a method to solve for the two parameters is provided.

6.1. Quasineutrality at the Debye sheath entrance

In general, solving equation (1.3) in the magnetic presheath is a numerical task. However, near the Debye sheath entrance the quasineutrality equation can be expanded to obtain analytical expressions relating the electric field to the distribution function in this region. This analysis is valid for $\sqrt{Zm_e/m_i} \ll \alpha$, as it assumes equation (3.12) for the electron density.

The variation in density in the magnetic presheath, close to the Debye sheath entrance, for both ions and electrons is related to the variation in the electrostatic potential, $\delta\phi(x) = \phi(x) - \phi_{\text{DSE}}$. The Boltzmann distribution (3.12) is expanded near the Debye sheath entrance to obtain

$$n_e(x) \simeq Z n_{\text{MPE}} \exp\left(\frac{e\phi_{\text{DSE}}}{T_e}\right) \left(1 + \frac{e\delta\phi}{T_e} + \left(\frac{e\delta\phi}{T_e}\right)^2\right). \quad (6.1)$$

For ions, the variation in density is obtained by following the characteristics of the ion motion backwards from the Debye sheath entrance, while ignoring additional ‘‘branches’’ of the trajectory arising due to the quasi-periodic motion that this trajectory exhibits further in the past (i.e. ignoring the contribution from closed orbits).[†] To lowest order in α , the orbit parameters \bar{x} and U_{\perp} are constant; in addition, the total energy U is exactly constant. Consider equations (4.10), (4.11) and (4.12) for the ion velocity in the magnetic presheath. The quantities v_z , $v_y + \Omega x$ and $-\sqrt{v_x^2 + 2\Omega\delta\phi(x)/B - 2\Omega^2\bar{x}x + \Omega^2x^2}$ are constant and, from equations (4.21), (4.19) and (4.23), are equal to the components of the velocity at the Debye sheath entrance. Thus, the ion density at a distance x from the wall, near the Debye sheath entrance, is

$$n_i(x) \simeq \int f_{\text{DSE}} \left(-\sqrt{v_x^2 + \frac{2\Omega\delta\phi(x)}{B}} - 2\Omega v_y x + \Omega^2 x^2, v_y + \Omega x, v_z \right) d^3v. \quad (6.2)$$

The quasineutrality equation (1.3) to lowest order in $e\delta\phi(x)/T_e \ll v_x^2/v_B^2$ and $x \ll v_x^2/(\Omega v_y) \sim v_x^2/(\Omega c_s)$ [‡] gives an equation for ϕ_{DSE} ,

$$n_{\text{MPE}} \exp\left(\frac{e\phi_{\text{DSE}}}{T_e}\right) \simeq \int f_{\text{DSE}}(\mathbf{v}) d^3v. \quad (6.3)$$

Since the electron density has no variation proportional to $\sqrt{\delta\phi}$, the ion density must not either and thus (Geraldini *et al.* 2018)

$$f_{\text{DSE}}(v_x = 0) = 0. \quad (6.4)$$

Ions reaching the Debye sheath entrance travelling tangentially to the wall are absent.

[†] In reference Geraldini *et al.* (2018) a more careful expansion of the ion density is performed.

[‡] For $v_y = \Omega\bar{x} \gg c_s$ the distribution function is exponentially small provided it is exponentially decaying at large energies, and therefore the typical value $v_y \sim c_s$ can be used.

Since no ions are coming out of the Debye sheath, these ions would have to have been travelling towards the wall at past times and would therefore have $\dot{v}_x \geq 0$ and, from equation (4.4), $v_y \geq \phi'(x)/B$. Recalling that $v_y \simeq \Omega\bar{x}$, one can always find ions with a sufficiently large value of \bar{x} such that $v_y \geq \phi'(x)/B$, if $\phi'(x)$ is finite. It therefore follows that, for ions with $v_x = 0$ to be absent, $\phi'(x)$ must be divergent at the Debye sheath entrance on the magnetic presheath scale.¶ As will be explicitly shown in section 6, this divergence causes the asymptotic distribution function f_{DSE} to decay exponentially for $v_x \rightarrow 0$ provided $F(\mu, U)$ decays exponentially for $U \rightarrow \infty$. Therefore, the first argument of f_{DSE} in (6.2) can be safely Taylor expanded.

Expanding equation (6.2) in $e\delta\phi(x)/T_e \ll v_x^2/v_B^2$ and $x \ll v_x^2/(\Omega c_s)$ gives

$$n_i(x) \simeq \int f_{\text{DSE}}(\mathbf{v})d^3v + \frac{\Omega\delta\phi}{B} \int \frac{f_{\text{DSE}}(\mathbf{v})}{v_x^2}d^3v - \frac{1}{2}\Omega x \int \frac{v_y f_{\text{DSE}}(\mathbf{v})}{v_x^2}d^3v + 3 \left(\frac{\Omega\delta\phi}{B}\right)^2 \int \frac{f_{\text{DSE}}(\mathbf{v})v_y}{v_x^4}d^3v, \quad (6.5)$$

where the term $\Omega^2 x^2 \ll 2\Omega^2 \bar{x}x$ was neglected. Note that the Taylor expansion of the second argument of f_{DSE} in equation (6.2), $v_y + \Omega x$, about v_y did not give a variation in x . Collecting higher order terms in the quasineutrality equation gives an equation relating electrostatic potential variation and position,

$$\frac{e\delta\phi}{T_e} \left(\int f_{\text{DSE}}(\mathbf{v})d^3v - v_B^2 \int \frac{f_{\text{DSE}}(\mathbf{v})}{v_x^2}d^3v \right) + \left(\frac{e\delta\phi}{T_e} \right)^2 \left(n_{i,\text{DSE}} - 3v_B^4 \int \frac{f_{\text{DSE}}(\mathbf{v})v_y}{v_x^4}d^3v \right) + \frac{1}{2}\Omega x \int \frac{f_{\text{DSE}}(\mathbf{v})v_y}{v_x^2}d^3v \simeq 0. \quad (6.6)$$

Since, as was concluded in the previous paragraph, the electric field must diverge for $x \rightarrow 0$, the appropriate balance in equation (6.6) is $\delta\phi^2 \propto x$. By setting the term linear in $\delta\phi$ to zero, we obtain the marginal form of the kinetic Bohm condition (Geraldini *et al.* 2018),

$$v_B^2 \int \frac{f_{\text{DSE}}(\mathbf{v})}{v_x^2}d^3v = \int f_{\text{DSE}}(\mathbf{v})d^3v, \quad (6.7)$$

Since (6.7) applies to the *lowest-order* distribution function in the region $\lambda_D \ll x \ll \rho_B$, it need not — and indeed will not (Riemann 2012; Baalrud & Hegna 2012) — apply to the exact distribution function measured near a target in an experiment.† Nonetheless, $f_{\text{DSE}}(\mathbf{v})$ is (within the validity of the underlying orderings) an approximation of the true distribution function in the region $\lambda_D \ll x \ll \rho_B$.

¶ The divergence in $\phi'(x)$ is resolved by retaining the term $\epsilon_0\phi''(x)$, small in $\lambda_D/\rho_s \ll 1$, in Poisson's equation (1.2).

† There are small corrections to the asymptotic distribution function $f_{\text{DSE}}(\mathbf{v})$ in the region $\lambda_D \ll x \ll \rho_B$. With a finite but large electric field, $\phi'(x)$, the distribution function in this region does not exactly satisfy $f(x, \mathbf{v}) = 0$ for $v_x = 0$, due to the small number of very high-energy ions whose bottom turning point lies in the Debye sheath. A very small number of ion collisions in this region, or ion reflection from the target, both neglected, would also cause $f(x, \mathbf{v}) \neq 0$ for $v_x \geq 0$. If the exact distribution function, $f(x, \mathbf{v})$, were used instead of the asymptotic one, $f_{\text{DSE}}(\mathbf{v})$, in the kinetic Bohm condition (6.7), then the left hand side would diverge, $\int (f(x, \mathbf{v})/v_x^2)d^3v \rightarrow \infty$, and the condition could not even be approximately satisfied.

Imposing (6.7), equation (6.6) becomes

$$\left(\frac{e\delta\phi}{T_e}\right)^2 \left(\int f_{\text{DSE}}(\mathbf{v}) d^3v - 3v_{\text{B}}^4 \int \frac{f_{\text{DSE}}(\mathbf{v})v_y}{v_x^4} d^3v \right) + \frac{1}{2}\Omega x \int \frac{f_{\text{DSE}}(\mathbf{v})v_y}{v_x^2} d^3v \simeq 0. \quad (6.8)$$

The electrostatic potential variation in the magnetic presheath, near the Debye sheath entrance, is thus given by

$$\frac{e(\phi(x) - \phi(0))}{T_e} \simeq \frac{\sqrt{2\bar{x}_{\text{av}}x}}{\rho_{\text{B}}}, \quad (6.9)$$

with \bar{x}_{av} , denoting a kinetic average of $\bar{x} = v_y/\Omega$, given by

$$\frac{\bar{x}_{\text{av}}}{\rho_{\text{B}}} = \frac{v_{\text{B}} \int (v_y f_{\text{DSE}}(\mathbf{v})/v_x^2) d^3v}{\int f_{\text{DSE}}(\mathbf{v}) (3v_{\text{B}}^4/v_x^4 - 1) d^3v} \sim \frac{\sqrt{1+\tau}}{(1+\alpha\tau)}. \quad (6.10)$$

Since f_{DSE} is exponentially small near $v_x = 0$, the integral in the denominator of (6.10) is convergent. The ordering in (6.10) can be obtained as follows. For $\alpha\tau \lesssim 1$, $v_x \sim v_{\text{B}}$ and $v_y \sim c_s$ lead to $\bar{x}_{\text{av}}/\rho_{\text{B}} \sim c_s/v_{\text{B}} \sim \sqrt{1+\tau}$. For $\alpha\tau \gg 1$, the ordering $v_x \sim \sqrt{\alpha\tau}v_{\text{B}}$ is incompatible with the kinetic Bohm condition (6.7) unless a number of “slow” ions, with small $|v_x|$, are present to increase the left hand side of (6.7) from the estimate $n_{\text{DSE}}/(\alpha\tau v_{\text{B}}^2)$ arising from most of the ions. From equation (6.2), the marginalized distribution function is ordered $\int f_{\text{DSE}} dv_y dv_z \sim n_{\text{DSE}}/(\sqrt{\alpha\tau}v_{\text{B}})$. Assuming the left hand side of (6.7) to be dominated by the contribution of slow ions, we obtain $\int (f_{\text{DSE}}/v_x^2) d^3v \sim (\int f_{\text{DSE}} dv_y dv_z)/v_x \sim 1/(\sqrt{\alpha\tau}v_{\text{B}}v_x)$. Thus, the slow ion velocity must be ordered $v_x \sim v_{\text{B}}/\sqrt{\alpha\tau}$. For $\alpha\tau \gg 1$, the slow ions dominate the integrals in (6.10) and thus, using $v_y \sim v_{\text{t},i}$, the estimate $\bar{x}_{\text{av}}/\rho_{\text{B}} \sim v_{\text{t},i}v_x^2/v_{\text{B}}^3 \sim \sqrt{\tau}/(\alpha\tau) \sim 1/(\alpha\tau^{1/2})$ is obtained.

The region of validity of equation (6.9) is obtained by investigating the validity of the expansion (6.6). In order for the expansion to be valid, the orderings $e\delta\phi(x)/T_e \ll v_x^2/v_{\text{B}}^2$ and $x \ll v_x^2/(\Omega c_s)$ must be satisfied. The distribution function exponentially decays at small values of v_x , and the smallest value of v_x which is possessed by a significant number of ions was ordered to be $v_x^2 \sim v_{\text{B}}^2/(1+\alpha\tau)$. Using $x \ll v_x^2/(\Omega c_s)$, the ordering $x \ll \rho_s/[(1+\tau)(1+\alpha\tau)]$ for the region of validity of the expansion is obtained. The same ordering results from $e\delta\phi(x)/T_e \ll v_x^2/v_{\text{B}}^2$ using equations (6.9) and (6.10).

6.2. Ion trajectories and ion distribution function for $\tau \gg 1$

In order to obtain $f_{\text{DSE}}(\mathbf{v})$ from (5.9), the electrostatic potential in the magnetic presheath is necessary to calculate the function $\chi_{\text{M}}(\bar{x})$ from equation (6.11), the function $\mu_{\text{op}}(\bar{x})$ from equation (4.20) and the quantities \bar{x}_c and ϕ_{DSE} from equation (4.18). These quantities are calculated here by analyzing ion trajectories for $\tau \gg 1$ in the electrostatic potential of equation (6.9).

For $\tau \gg 1$, the thermal velocity of an ion is much larger than the Bohm velocity, $v_{\text{t},i}^2 \sim \tau v_{\text{B}}^2 \gg v_{\text{B}}^2$. To calculate the adiabatic invariant, we can therefore neglect the small electrostatic potential variation throughout the orbit, $\Omega\phi(x)/B \sim v_{\text{B}}^2 \ll \Omega\mu_{\text{op}}(\bar{x}) \sim v_{\text{t},i}^2$, and using equation (4.20) obtain $\mu_{\text{op}}(\bar{x}) \simeq \chi_{\text{M}}(\bar{x})/\Omega$. This does not specify the functional form of $\mu_{\text{op}}(\bar{x})$ and $\chi_{\text{M}}(\bar{x})$, but in relating them reduces the number of unknown functions from two to one. Considering that ions reaching the wall have $U_{\perp} \simeq \chi_{\text{M}}(\bar{x})$, the equivalence of U_{\perp} and $\Omega\mu$ and the conservation of U and μ imply that the ion velocity parallel to the magnetic field, $V_{\parallel}(U_{\perp}, U) = \sqrt{2(U - U_{\perp})}$, has not changed from its value at the magnetic presheath entrance, $\sqrt{2(U - \Omega\mu)}$. Thus, in the model the ion tangential velocity is influenced by the electric field exclusively in the $\mathbf{E} \times \mathbf{B}$ (i.e., y) direction. The

quantity \bar{x}_c , defined in (4.18), corresponds to the smallest value of orbit position of an infinitesimally small gyro-orbit; no periodic solutions to lowest order in $\alpha \ll 1$ exist for even smaller values of \bar{x} . The smallest orbit has zero adiabatic invariant, and thus \bar{x}_c is obtained through $\mu_{\text{op}}(\bar{x}_c) = 0$.

When an ion in a large gyro-orbit gets sufficiently close to the target its gyro-motion is distorted, as shown in figure 1(b). The net force away from the wall on an ion at a given instant is given by the effective potential gradient, $\chi'(x, \bar{x})$. The distortion of ion gyro-orbits is caused by a balance of the magnetic force pulling away from the wall and the electric force pushing towards the wall. This balance occurs at the location of the effective potential maximum x_M , which is obtained from $\chi'(x_M, \bar{x}) = 0$ (the analogue of equation (4.14)),

$$\chi'(x_M, \bar{x}) = \Omega^2(x_M - \bar{x}) + \frac{\Omega\phi'(x_M)}{B} = 0. \quad (6.11)$$

In what follows, the electrostatic potential in (6.9) is used to approximate the electrostatic potential at distances from the wall corresponding to typical values of x_M . The resulting values of x_M , however, will be shown to be too large to be within the region of validity of equation (6.9), but numerical results will show that this analysis is nonetheless a good approximation for $\tau \gg 1$. From (6.9) we obtain $\phi'(x_M) = (T_e/e\rho_B)\sqrt{\bar{x}_{\text{av}}/2x_M}$, and using the ordering $x_M \ll \bar{x} \sim \phi'(x_M)/\Omega B \sim \rho_i$ and equation (6.11), we obtain

$$x_M = \frac{\bar{x}_{\text{av}}\rho_B^2}{2\bar{x}^2}. \quad (6.12)$$

Hence, using $\bar{x} \sim \rho_s \sim \rho_i$ and $\bar{x}_{\text{av}} \sim \rho_i/(1 + \alpha\tau)$ for $\tau \gg 1$, it follows that $x_M \sim \rho_i/[\tau(1 + \alpha\tau)]$. Since the expansion used to derive equation (6.9) is valid, for $\tau \gg 1$, in the region $x_M \ll \rho_i/[\tau(1 + \alpha\tau)]$, the effective potential maximum lies in a region where the form of the electrostatic potential used to derive its position is not valid.

By inserting (6.12) into $\chi_M(\bar{x}) = \Omega^2(x_M - \bar{x})^2/2 + \Omega\phi(x_M)/B$, neglecting the term $\Omega^2x_M^2/2$ and remembering that $\mu_{\text{op}}(\bar{x}) \simeq \chi_M(\bar{x})/\Omega$, we obtain

$$\Omega\mu_{\text{op}}(\bar{x}) \simeq \chi_M(\bar{x}) \simeq \frac{1}{2}\Omega^2\bar{x}^2 + \frac{v_B^2\bar{x}_{\text{av}}}{2\bar{x}} + \frac{\Omega\phi_{\text{DSE}}}{B}. \quad (6.13)$$

Imposing $\mu_{\text{op}}(\bar{x}_c) = 0$ in equation (6.13) gives

$$\bar{x}_c = \rho_B \sqrt{-\frac{2e\phi_{\text{DSE}}}{T_e} - \frac{v_c^2}{v_B^2}} \quad (6.14)$$

where a new quantity, called the critical velocity $v_c = v_B\sqrt{\bar{x}_{\text{av}}/\bar{x}_c}$, is introduced such that \bar{x}_{av} is given by

$$\bar{x}_{\text{av}} = \frac{v_c^2}{v_B^2}\bar{x}_c. \quad (6.15)$$

The critical velocity is the value of $|v_x|$ for a particle with $\mu = 0$, which came from an infinitesimally small gyro-orbit, reaching the Debye sheath entrance. Such ions have $\bar{x} = \bar{x}_c$ and $\chi_M(\bar{x}_c) - \Omega^2\bar{x}^2/2 - \Omega\phi_{\text{DSE}}/B = v_B^2\bar{x}_{\text{av}}/2\bar{x} = v_c^2/2$. In theory these infinitesimally small ions should have $\mu'_{\text{op}}(\bar{x}_c) = 0$ and thus $\Delta_M(\bar{x}_c, U) = 0$ for all values of U , and this would give $v_x = -v_c$ as the only allowed value according to the velocity distribution (5.9). However, since the model does not correctly capture the small gyro-orbits[†], which

[†] Although not as evidently, the asymptotic theory is also inaccurate for small gyro-orbits. This inaccuracy is unimportant if τ is sufficiently large that the asymptotic theory correctly

are heavily affected by the electric field, ions with $\mu = 0$ in the model have a finite range of velocities due to the fact that $\mu'_{\text{op}}(\bar{x}_c) = 0$ is not imposed (otherwise the model would be overconstrained, unless additional parameters are introduced). It can be shown that $\mu'_{\text{op}}(\bar{x}_c) > 0$ is always satisfied in the model for α sufficiently small that $|\ln \alpha| \gg 1$. From equation (6.13), $\mu'_{\text{op}}(\bar{x}_c) = \Omega \bar{x}_c - v_c^2 / (2\Omega \bar{x}_c)$, implying that $\mu'_{\text{op}}(\bar{x}_c) > 0$ provided that $2(\Omega \bar{x}_c)^2 > v_c^2$. Using $e|\phi_{\text{DSE}}|/T_e \sim \ln \alpha$, from equation (6.14) we obtain $2(\Omega \bar{x}_c)^2 \sim |\ln \alpha| v_{\text{B}}^2$, which is larger than $v_c^2 \sim v_{\text{B}}^2$ for sufficiently small α . With $\mu'_{\text{op}}(\bar{x}_c) > 0$, according to equation (4.23) ions with $\mu = 0$ ($\bar{x} = \bar{x}_c$) have a non-zero range of values of v_x . Therefore, in the model $|v_x| = v_c$ is the smallest value of $|v_x|$ for an ion with $\mu = 0$. Although $\mu'_{\text{op}}(\bar{x}_c) \neq 0$ may look like a serious shortcoming of the model, for $\tau \gg 1$ the large discrepancy in the function $\mu'_{\text{op}}(\bar{x})$ is expected only for a small number of particles near $\bar{x} = \bar{x}_c$.

From equations (6.13) and (4.23), large gyro-orbits at the Debye sheath entrance have a range of normal velocities given by

$$\frac{v_c^2 \bar{x}_c}{2\bar{x}} \leq \frac{v_x^2}{2} < \frac{v_c^2 \bar{x}_c}{2\bar{x}} + 2\pi\alpha\mu'_{\text{op}}(\bar{x})\sqrt{2(U - \Omega\mu_{\text{op}}(\bar{x}))}. \quad (6.16)$$

Inserting the velocity spread (6.16) in the distribution function (5.9) the velocity distribution of ions in large gyro-orbits is

$$f_{\text{DSE}}(v_x, v_y, v_z) \simeq F(\mu_{\text{op}}(\bar{x}), U) \Theta(\bar{x} - \bar{x}_c) \Theta(-v_x) \\ \times \hat{H}\left(\frac{1}{2}v_x^2 - \frac{v_c^2 \bar{x}_c}{2\bar{x}}, 0, 2\pi\alpha\mu'_{\text{op}}(\bar{x})\sqrt{2(U - \Omega\mu_{\text{op}}(\bar{x}))}\right). \quad (6.17)$$

The only unknowns that specify the model distribution function (6.17) are the two constants ϕ_{DSE} and v_c . The value of ϕ_{DSE} is determined from quasineutrality at the Debye sheath entrance, equation (6.3). The value of v_c is determined by imposing the kinetic Bohm condition (6.7).

6.3. Model closure: calculating ϕ_{DSE} and v_c

For numerical evaluation, it is best to re-express all velocity moments as

$$\int f_{\text{DSE}}(\mathbf{v})v_x^a d^3v = \int_{\bar{x}_c}^{\infty} \Omega d\bar{x} \int_{\Omega\mu_{\text{op}}(\bar{x})}^{\infty} F\left(\mu_{\text{op}}(\bar{x}), \Omega\mu_{\text{op}}(\bar{x}) + \frac{1}{2}v_z^2\right) \\ \times \frac{v_c^{a+1}}{a+1} \left(\left(\frac{\bar{x}_c}{\bar{x}} + \frac{4\pi\alpha\mu'_{\text{op}}(\bar{x})v_z}{v_c^2}\right)^{(a+1)/2} - \left(\frac{\bar{x}_c}{\bar{x}}\right)^{(a+1)/2} \right) dv_z,$$

obtained from (6.17) using the change of variables $v_y = \Omega\bar{x}$ and $v_z = \sqrt{2(U - \Omega\mu_{\text{op}}(\bar{x}))}$, and substituting (6.15). In particular, to solve equations (6.3) and (6.7) for ϕ_{DSE} and v_c , we require the density,

$$n_{\text{DSE}} = \int f_{\text{DSE}}(\mathbf{v})d^3v = \int_{\bar{x}_c}^{\infty} \Omega d\bar{x} \int_{\Omega\mu_{\text{op}}(\bar{x})}^{\infty} F\left(\mu_{\text{op}}(\bar{x}), \Omega\mu_{\text{op}}(\bar{x}) + \frac{1}{2}v_z^2\right) \\ \times \left(\left(\frac{\bar{x}_c}{\bar{x}} + \frac{4\pi\alpha\mu'_{\text{op}}(\bar{x})v_z}{v_c^2}\right)^{1/2} - \left(\frac{\bar{x}_c}{\bar{x}}\right)^{1/2} \right) dv_z, \quad (6.18)$$

describes the majority of ion orbits. It was shown in Geraldini *et al.* (2019) that only when $\tau \lesssim \alpha^{1/3}$, the asymptotic theory fails for most ions.

and the Bohm integral,

$$I_{\text{Bohm}} = \int \frac{f_{\text{DSE}}(\mathbf{v})}{v_x^2} d^3v = \int_{\bar{x}_c}^{\infty} \Omega d\bar{x} \int_{\Omega\mu_{\text{op}}(\bar{x})}^{\infty} F\left(\mu_{\text{op}}(\bar{x}), \Omega\mu_{\text{op}}(\bar{x}) + \frac{1}{2}v_z^2\right) \times \frac{1}{v_c} \left(\left(\frac{\bar{x}_c}{\bar{x}}\right)^{-1/2} - \left(\frac{\bar{x}_c}{\bar{x}} + \frac{4\pi\alpha\mu'_{\text{op}}(\bar{x})v_z}{v_c^2}\right)^{-1/2} \right) dv_z. \quad (6.19)$$

Note that the value of I_{Bohm} decreases by increasing v_c , and vice versa.

Iterative expressions are used to determine ϕ_{DSE} from equation (6.3) and v_c from equation (6.7). Using (6.18), equation (6.3) is re-expressed to $\phi_{\text{DSE}} = (T_e/e) \ln(n_{\text{DSE}}/n_{\text{MPE}})$. Using (6.19), equation (6.7) is re-expressed to $I_{\text{Bohm}} = n_{\text{DSE}}/v_{\text{B}}^2$. The first guesses, or zeroth iterates, are defined by $\phi_{\text{DSE},0} = (T_e/e) \ln \alpha$ and $v_{c,0} = v_{\text{B}}$, and iteration values are denoted by $\phi_{\text{DSE},\nu}$ and $v_{c,\nu}$. At each iteration, $n_{\text{DSE},\nu}$ and $I_{\text{Bohm},\nu}$ are evaluated from equations (6.18) and (6.19). The iterates $\phi_{\text{DSE},\nu+1}$ and $v_{c,\nu+1}$ are obtained using

$$\phi_{\text{DSE},\nu+1} = \frac{T_e}{e} \ln\left(\frac{n_{\text{DSE},\nu}}{n_{\text{MPE}}}\right), \quad (6.20)$$

$$v_{c,\nu+1} = \frac{v_{c,\nu}}{I_{\text{Bohm},\nu}} \left(I_{\text{Bohm},\nu} - \frac{n_{\text{DSE},\nu}}{v_{\text{B}}^2} \right) \quad \text{if } I_{\text{Bohm},\nu} > \frac{n_{\text{DSE},\nu}}{v_{\text{B}}^2} \\ = \epsilon_{v_c} \quad \text{else,} \quad (6.21)$$

and the iteration is truncated when

$$\frac{n_{\text{DSE},N} - n_{\text{DSE},N-1}}{n_{\text{DSE},N}} < \epsilon_n, \quad (6.22)$$

$$\left| \frac{v_{\text{B}}^2 I_{\text{Bohm},N}}{n_{\text{DSE},N}} - 1 \right| < \epsilon_I. \quad (6.23)$$

Note that equation (6.21) is based on a Newton method with the approximations $dn_{\text{DSE}}/dv_c \approx 0$ and $dI_{\text{Bohm}}/dv_c \approx -I_{\text{Bohm}}/v_c$. In the earliest iterations, it may happen that $v_{c,\nu+1} \leq 0$, which is prevented by setting $v_{c,\nu+1}$ to be a small number above zero (smaller than the solution v_c), denoted ϵ_{v_c} . The N th iteration values of ϕ_{DSE} and v_c , satisfying conditions (6.22) and (6.23), are considered to be acceptable numerical solutions of (6.3) and (6.7). The value of \bar{x}_{av} is obtained from v_c using equation (6.15). To obtain the results presented in the next section, $\epsilon_n = \epsilon_I = \epsilon_{v_c} = 10^{-10}$ was used.

Having solved equations (6.3) and (6.7) for ϕ_{DSE} and $v_c = v_{\text{B}}\sqrt{\bar{x}_{\text{av}}/\bar{x}_c}$, equations (4.19), (4.21), (6.13), (6.14) and (6.17) completely specify the large gyro-orbit model distribution function at the Debye sheath entrance, $f_{\text{DSE}}(\mathbf{v})$. The model distribution function at the wall is obtained by replacing equation (6.17) with

$$f_{\text{W}}(\mathbf{v}) \simeq F(\mu_{\text{op}}(\bar{x}), U) \Theta(\bar{x} - \bar{x}_c) \Theta(-v_x) \\ \times \hat{\Pi} \left(\frac{1}{2}v_x^2 - \frac{v_c^2\bar{x}_c}{2\bar{x}} - \frac{\Omega}{B} (\phi_{\text{DSE}} - \phi_{\text{W}}), 0, 2\pi\alpha\Omega\bar{x}\sqrt{2(U - \Omega\mu_{\text{op}}(\bar{x}))} \right), \quad (6.24)$$

where equation (5.8) determines the wall potential ϕ_{W} .

6.4. Reduced model

Consider equation (6.13) for $\chi_{\text{M}}(\bar{x})$. For $\alpha\tau \gg 1$, the term $v_{\text{B}}^2\bar{x}_{\text{av}}/(2\bar{x}) \sim v_{\text{B}}^2/(\alpha\tau) \ll v_{\text{B}}^2$ is so small that it can be neglected by setting $\bar{x}_{\text{av}} = v_c = 0$. In this case, the distribution function at the Debye sheath entrance is similar to the one calculated by

Parks & Lippmann (1994) at the target (though their paper is for general α). With $v_c = 0$, the constraint provided by the Bohm condition (6.7) must be dropped. The reduced model for the distribution function at the Debye sheath entrance, $f_{\text{DSE}}(\mathbf{v})$, consists of the equations (4.19), (4.21), (6.3), (6.13), (6.14) and (6.17). The iteration scheme to solve the reduced model is the same as in the previous subsection, with $v_c = 0$ replacing all equations involving v_c . To calculate the wall velocity distribution, equations (6.24) and (5.8) are also required.

7. Numerical results

In this section, a comparison is presented of numerical results obtained using the full asymptotic theory (i) and the large gyro-orbit model (ii). To obtain the solutions (i), the numerical scheme in Geraldini *et al.* (2018), which solves for $\phi(x)$ to obtain $f_{\text{DSE}}(\mathbf{v})$, is used. In section 7.1 the boundary conditions for the distribution function at the magnetic presheath entrance, as a function of τ , are introduced. Then, in section 7.2, results for the distribution of the wall-normal velocity component, v_x , at the Debye sheath entrance obtained using (i) and (ii) are presented. A narrowing of the distribution function for decreasing values of α is explained, and the approximate validity of the large gyro-orbit model for $\tau \gg 1$ is justified, as well as the qualitative validity of the model for $\tau \sim 1$. Finally, results for the energy-angle distributions of ions at the wall are presented in section 7.3 for some values of α and τ . A crude extension to the model for $\alpha \sim \sqrt{Zm_e/m_i}$ is suggested in section 7.4.

7.1. Boundary conditions at the magnetic presheath entrance

The ion velocity distribution at the magnetic presheath entrance, $\rho_s \ll x \ll d_c$, is taken to be

$$f_{\text{MPE}}(\mathbf{v}) = \begin{cases} \mathcal{N} n_{\text{MPE}} \frac{4v_z^2}{\pi^{3/2} v_{t,i}^5} \exp\left(-\frac{|\mathbf{v} - uv_{t,i}\hat{\mathbf{e}}_z|^2}{v_{t,i}^2}\right) \Theta(v_z) & \text{for } \tau \leq 1, \\ \mathcal{N} n_{\text{MPE}} \frac{4v_z^2}{\pi^{3/2} v_{t,i}^3 (v_{t,i}^2 + \tau v_z^2)} \exp\left(-\frac{|\mathbf{v}|^2}{v_{t,i}^2}\right) \Theta(v_z) & \text{for } \tau > 1, \end{cases} \quad (7.1)$$

for any prescribed value of τ , where Θ is the Heaviside step function defined in (3.6) and $\hat{\mathbf{e}}_z$ is a unit vector in the z direction. The family of velocity distributions (7.1) is the same used in Geraldini *et al.* (2019) to study the dependence of the magnetic presheath solution on ion temperature, and is chosen to satisfy the marginal kinetic Chodura condition

$$v_B^2 \int \frac{f_{\text{MPE}}(\mathbf{v})}{v_z^2} d^3v = n_{\text{MPE}}. \quad (7.2)$$

Equation (7.2) is the marginal form of an existence condition for steady state solutions of $\phi(x)$ at the magnetic presheath entrance; thus, it is a necessary condition for the existence of steady state solutions of $\phi(x)$ in the magnetic presheath (Geraldini *et al.* 2018). The value of the normalization constant \mathcal{N} is obtained from (5.4), giving

$$\mathcal{N} = \begin{cases} \left[(1 + 2u^2) (1 + \text{erf}(u)) + \frac{2u}{\sqrt{\pi}} \exp(-u^2) \right]^{-1} & \text{for } \tau \leq 1, \\ r^{3/2} \left[2\sqrt{r} - 2\sqrt{\pi} \exp\left(\frac{1}{r}\right) \left(1 - \text{erf}\left(\frac{1}{\sqrt{r}}\right)\right) \right]^{-1} & \text{for } \tau > 1. \end{cases} \quad (7.3)$$

The values of u and r are obtained by imposing (7.2), leading to

$$1 + \text{erf}(u) = \tau \left[(1 + 2u^2) (1 + \text{erf}(u)) + \frac{2u}{\sqrt{\pi}} \exp(-u^2) \right], \quad (7.4)$$

$$r\sqrt{\pi} \exp\left(\frac{1}{r}\right) \left(1 - \operatorname{erf}\left(\frac{1}{\sqrt{r}}\right)\right) = \tau \left[2\sqrt{r} - 2\sqrt{\pi} \exp\left(\frac{1}{r}\right) \left(1 - \operatorname{erf}\left(\frac{1}{\sqrt{r}}\right)\right)\right]. \quad (7.5)$$

7.2. Narrowing of the wall-normal velocity distributions

The marginalized distribution function

$$f_{x,\text{DSE}}(v_x) = \int \int f_{\text{DSE}}(\mathbf{v}) dv_y dv_z, \quad (7.6)$$

is the distribution of wall-normal velocities v_x of ions at the Debye sheath entrance. The numerical results obtained for $f_{x,\text{DSE}}(v_x)$ with the model and the theory for $\tau = 1$ and $\tau = 5$, for a number of angles α , are shown in figure 3. The first thing to note is that the model distribution function (ii) (dashed lines) captures the essential features of the distribution function obtained from the full asymptotic theory (i) (solid lines). Moreover, the agreement is better for the largest value of $\tau = T_i/(ZT_e)$, $\tau = 5$. This is expected because the model is derived assuming that gyro-orbits are approximately circular until just before they reach the target, an assumption which is good if the ion temperature T_i is large enough that changes in the ion electrostatic potential energy of $\sim ZT_e = T_i/\tau$ only weakly affect the ion motion.

The width of the function $f_{x,\text{DSE}}(v_x)$ narrows as α decreases, a feature that was observed in Geraldini *et al.* (2018). The width of this function can be quantified using the variance $\langle \tilde{v}_x^2 \rangle$, defined using the second moment of $f_{x,\text{DSE}}(v_x)$,

$$\langle \tilde{v}_x^2 \rangle = \sqrt{\frac{\int m_i(v_x - u_{x,\text{DSE}})^2 f_{x,\text{DSE}}(v_x) dv_x}{\int f_{x,\text{DSE}}(v_x) dv_x}}, \quad (7.7)$$

where

$$u_{x,\text{DSE}} = \frac{\int v_x f_{x,\text{DSE}}(v_x) dv_x}{\int f_{x,\text{DSE}}(v_x) dv_x} \quad (7.8)$$

is the average wall-normal velocity at the Debye sheath entrance. As can be seen in figure 3, the variance of the distribution function scales linearly with α .

The scaling of the variance can be explained as follows. The ion velocity can be decomposed into two pieces: a piece coming from the electric field acceleration which depends only on \bar{x} (or μ), $V_{x,\text{slow}}(\bar{x}) = \sqrt{2(\chi_M(\bar{x}) - \Omega^2 \bar{x}^2/2 - \Omega \phi_{\text{DSE}}/B)}$, and an additional gyrophase dependent piece which gives the velocity range in (4.23). In figure 4 the behaviour of the function $V_{x,\text{slow}}(\bar{x})$ as a function of $\mu_{\text{op}}(\bar{x})$ is shown for some values of τ and α . The slow decay of $V_{x,\text{slow}}$ with μ is approximately captured by the model for $\tau = 5$, and for $(\tau, \alpha) = (1, 5^\circ)$. For $(\tau, \alpha) = (1, 1^\circ)$, the dependence of $V_{x,\text{slow}}$ on μ is stronger than predicted by the model, but is nonetheless fairly weak. Since the electric field accelerates the normal component of most ions to a similar value, the distribution function sharply drops to zero below this value, around $|v_x| \approx V_{x,\text{slow}}(\rho_s)$, a feature common to all velocity distributions in figure 3. The dominant contribution to the variance $\langle \tilde{v}_x^2 \rangle$ therefore comes from the range of allowed values of $|v_x|$ for given values of \bar{x} and U . For $\tau \gtrsim 1$, we order $\Omega \mu_{\text{op}} \sim \Omega^2 \bar{x}^2/2 \sim v_{t,i}^2$ and $\sqrt{2(U - \Omega \mu_{\text{op}}(\bar{x}))} \sim v_{t,i}$, and obtain the range of values of v_x^2 in (4.23) as $2\pi\alpha\mu'_{\text{op}}(\bar{x})\sqrt{2(U - \Omega \mu_{\text{op}}(\bar{x}))} \sim 2\pi\alpha v_{t,i}^2$. Hence, we recover the variance $\langle \tilde{v}_x^2 \rangle \sim \alpha v_{t,i}^2 \sim \alpha \tau v_B^2$ seen in the numerical results. The weak dependence of $V_{x,\text{slow}} \lesssim v_B$ on μ does not cause a significant contribution to $\langle \tilde{v}_x^2 \rangle$ unless $\alpha\tau$ is extremely small, seen in the numerical results of figure 3 as a saturation of the decrease of the variance for $\alpha \lesssim 1^\circ$.

When deriving the scaling of equation (6.10) for $\alpha\tau \gg 1$, the typical value of $|v_x|$ of

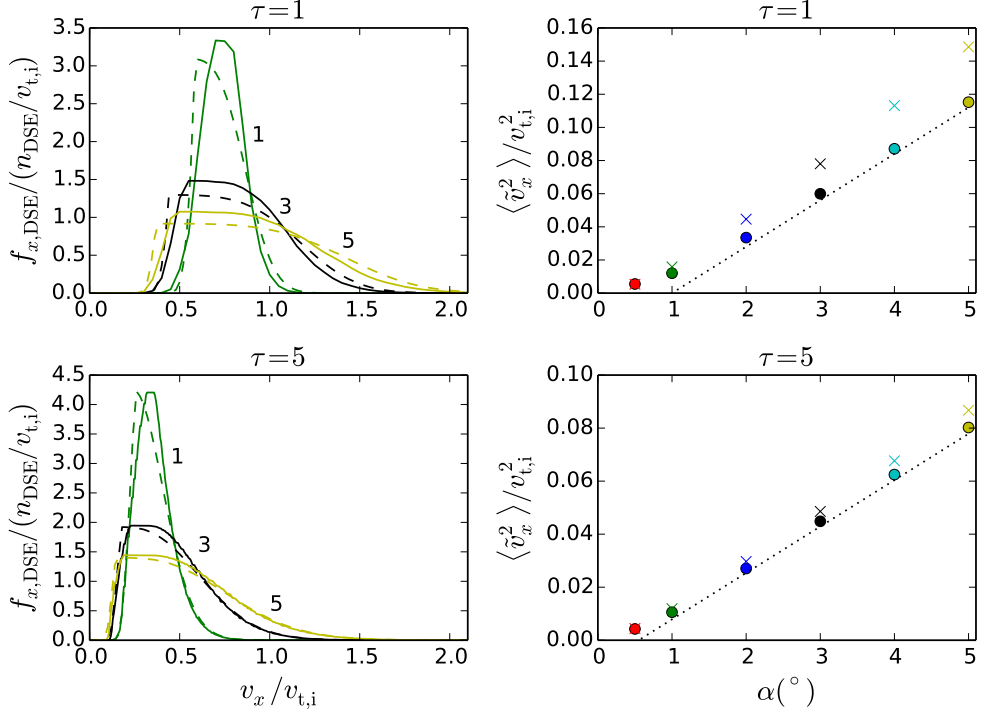


FIGURE 3. Left: wall-normal velocity distributions at the Debye sheath entrance from the theory (solid lines) and the large gyro-orbit model (dashed lines), for $\tau = 1$ (top) and $\tau = 5$ (bottom) for angles $\alpha = 1^\circ, 3^\circ, 5^\circ$. Right: the variance $\langle \tilde{v}_x^2 \rangle$ of the distributions from the theory (circles) and from the model (crosses) for values of α between 0.5° and 5° . The dotted lines are drawn to guide the eye, showing the linear scaling $\langle \tilde{v}_x^2 \rangle / v_{t,i}^2 \sim \alpha$ for $\alpha \gtrsim 1^\circ$. (Note: here α is measured in degrees.)

the slowest ions was found to be $V_{x,\text{slow}}(\rho_i) \sim v_B / \sqrt{\alpha\tau}$. From figure 4 it appears that the ordering $\alpha\tau \gtrsim 1$ is satisfied, as $V_{x,\text{slow}}(\bar{x})$ is smaller than v_B in most cases shown here. It may appear surprising that $V_{x,\text{slow}}/v_B$ is quite small also for $(\tau, \alpha) = (1, 5^\circ)$, as this suggests that $\alpha\tau$ is large for $\tau = 1$ and for a value of α ($= 5^\circ \approx 0.09$ radians) which is considered small. This observation prompts a closer analysis of the validity of the asymptotic theory of the ion orbits, which assumes $\alpha \ll 1$. One of the consequences of this ordering is that the function $\Delta_M(\bar{x}, U)$ is small. However, the smallness of $\Delta_M(\bar{x}, U)$ is measured relative to the total kinetic energy of the ion, estimated from the tangential components of the ion velocity, $(v_y^2 + v_z^2)/2 \sim (\Omega^2 \bar{x}^2 + v_{t,i}^2)/2$. The ratio $2\bar{\Delta}_M/(\Omega^2 \bar{x}^2 + v_{t,i}^2)$ is shown in figure 5 and highlights that, although for $\alpha = 5^\circ$ the validity of the asymptotic theory is not robust, the contribution of Δ_M to the ion energy is smaller than the total kinetic energy for most ions, albeit by a factor of ~ 2 only. Note that $\alpha = 5^\circ$ corresponds to $2\pi\alpha \approx 0.6$ radians, and so the factor of 2π in equation (4.22) explains why the expansion in α starts to become inaccurate at $\alpha \approx 5^\circ$.

Although the results of this subsection are for ion distribution functions at the Debye sheath entrance, $f_{x,DSE}(\mathbf{v})$, the validity of the scaling $\langle \tilde{v}_x^2 \rangle \sim \alpha v_{t,i}^2$ applies also to the ion velocity distribution at the wall, $f_{x,W}(\mathbf{v})$. However, at small enough values of α we obtain $\phi_{DSE} < \phi_W$, signalling that the ordering $\sqrt{Zm_e/m_i} \ll \alpha$, necessary to assume adiabatic electrons, is broken (recall equation (3.14)). In the next subsection, ion velocity

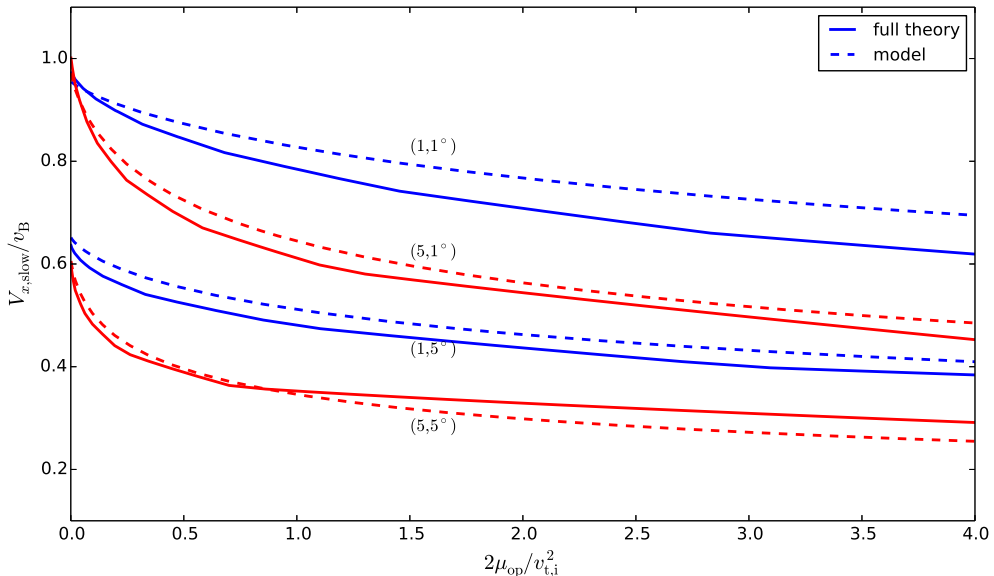


FIGURE 4. The smallest possible value of the normal velocity of an ion at the magnetic presheath entrance, $V_{x,\text{slow}}(\bar{x}) = \sqrt{2(\chi_M(\bar{x}) - \Omega^2 \bar{x}^2/2 - \Omega \phi_{\text{DSE}}/B)}$, is shown as a function of the adiabatic invariant $\mu_{\text{op}}(\bar{x})$ for with (τ, α) labelled. Solid lines correspond to the full asymptotic solution; dashed lines correspond to the large gyro-orbit model.

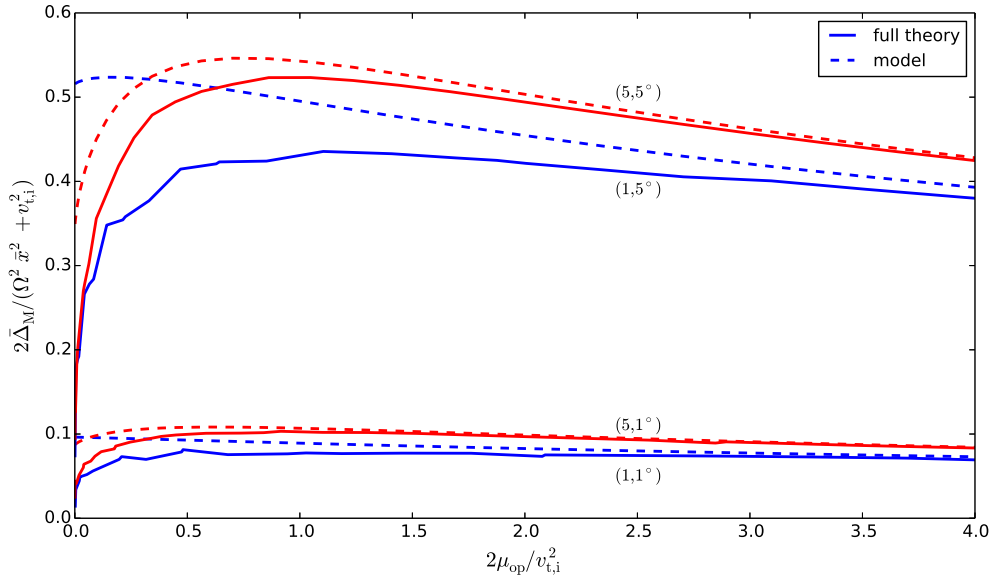


FIGURE 5. The quantity $2\bar{\Delta}_M/(\Omega^2 \bar{x}^2 + v_{t,i}^2)$, with $\bar{\Delta}_M(\bar{x}) = 2\pi\alpha\mu'_{\text{op}}(\bar{x})v_{t,i}$, is shown as a function of the adiabatic invariant $\mu_{\text{op}}(\bar{x})$ for labelled values of (τ, α) . Solid lines correspond to the full asymptotic solution; dashed lines correspond to the large gyro-orbit model. For $2\bar{\Delta}_M/(\Omega^2 \bar{x}^2 + v_{t,i}^2) \ll 1$ the asymptotic theory is valid.

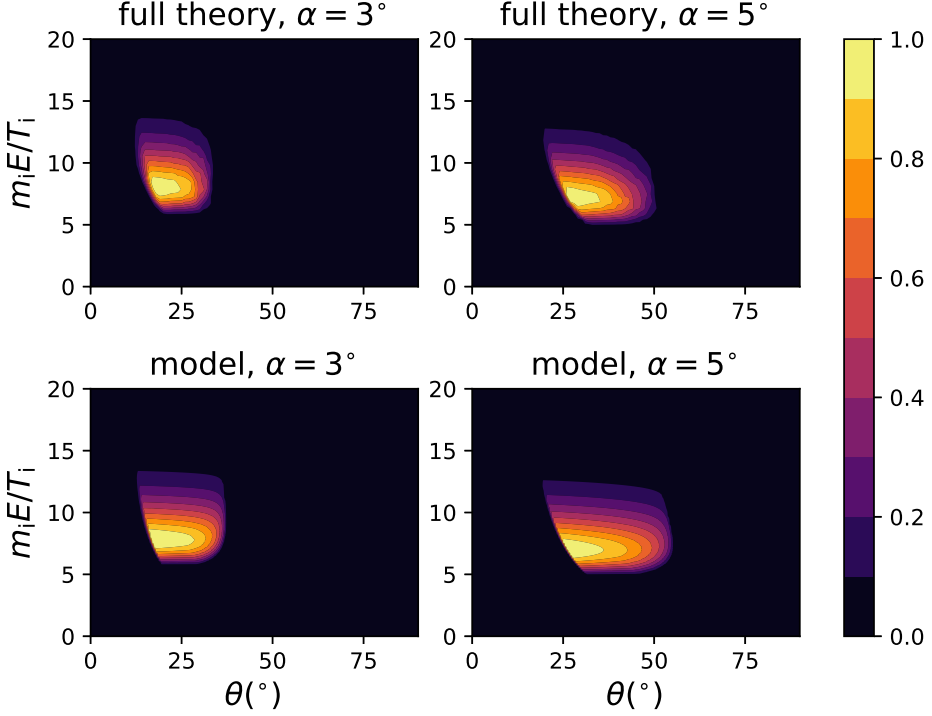


FIGURE 6. Energy-angle distributions at the target, $\zeta_W(E, \theta)$, obtained from the full asymptotic theory and from the large gyro-orbit model for $\tau = 0.5$ and $\alpha = 3^\circ$ and 5° , are shown normalized to their peak value.

distributions at the wall are considered for parameters where $\phi_{DSE} > \phi_W$, such that the assumption of Boltzmann electrons remains at least approximately correct.

7.3. Energy-angle distributions at the target

Since sputtering predictions depend on the distribution of kinetic energy and angle of impact of ions reaching the target, it is useful to calculate the energy-angle distribution of ions at the wall.

The kinetic energy of an ion at the wall is $E = U - \Omega\phi_W/B$ and the angle of impact of an ion with the wall surface is $\sin\theta = |v_x|/\sqrt{2E}$. Thus, the components v_z and v_x of the ion velocity can be expressed as functions of \bar{x} , E and θ via

$$v_x = -\sqrt{2E} \sin\theta, \quad (7.9)$$

$$v_z = \sqrt{2 \left(E - \chi_M(\bar{x}) + \frac{\Omega\phi_W}{B} \right)}. \quad (7.10)$$

The energy-angle distribution $\zeta_W(E, \theta)$ is calculated from $f_W(\mathbf{v})$ using the equation

$$\zeta_W(E, \theta) = \int_{\bar{x}_c}^{\chi_M^{-1}(E + \Omega\phi_W/B)} \frac{\sqrt{2E} \cos\theta}{\sqrt{2(E - \chi_M(\bar{x}) - \Omega\phi_W/B)}} f_W(\mathbf{v}) \Omega d\bar{x} \quad (7.11)$$

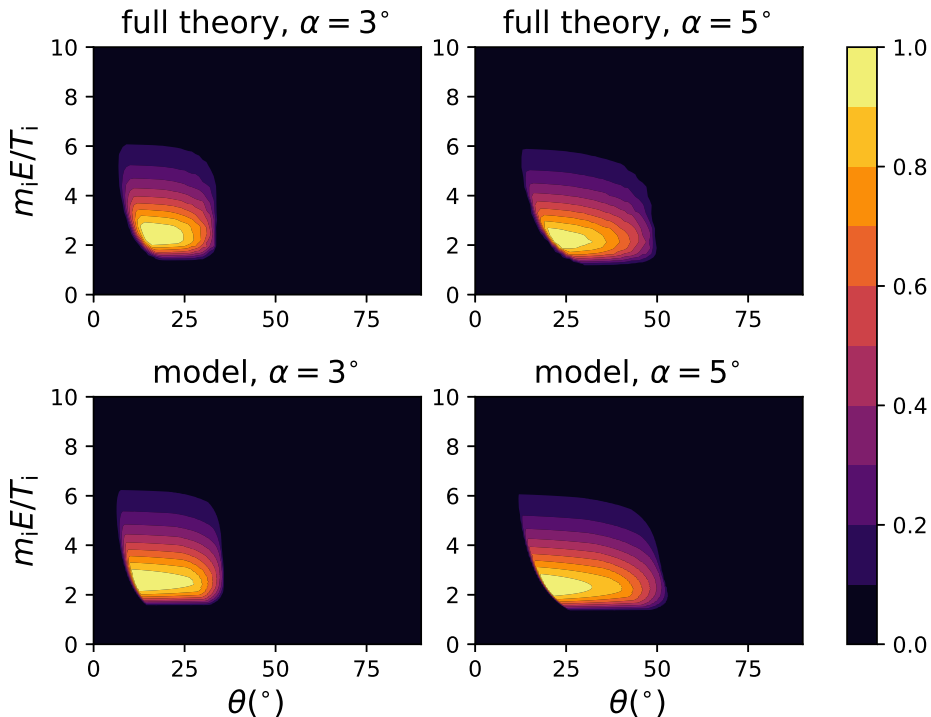


FIGURE 7. Energy-angle distributions at the target, $\zeta_W(E, \theta)$, obtained from the full asymptotic theory and from the large gyro-orbit model for $\tau = 2$ and $\alpha = 3^\circ$ and 5° , are shown normalized to their peak value.

where the Jacobian

$$\frac{\partial(v_x, v_z)}{\partial(E, \theta)} = \frac{\sqrt{2E} \cos \theta}{\sqrt{2(E - \chi_M(\bar{x}) + \Omega\phi_W/B)}} \quad (7.12)$$

was used to change variables from v_x and v_z to E and θ . The inverse function of $\chi_M(\bar{x})$, denoted χ_M^{-1} , is used to obtain the maximum value of \bar{x} for a given value of E , which is, from equation (7.10), the solution of $\chi_M(\bar{x}) = E + \Omega\phi_W/B$.

The energy-angle distributions calculated from the numerical solution of the full asymptotic theory (i) and from the large gyro-orbit model (ii) are shown for $\alpha = 3^\circ$ and 5° , for $\tau = 0.5$ — in figure 6 — and for $\tau = 2$ — in figure 7. The qualitative features of the distribution function obtained from the theory are, even for $\tau = 0.5$, adequately captured by the model, including the average angle of impact of ions with the wall. The model reproduces the distribution obtained from the asymptotic theory better at the largest of the two values of τ ($\tau = 2$, figure 7), as expected.

7.4. Accounting for $\sqrt{Zm_e/m_i} \sim \alpha$

For some of the angles we have considered, the assumption of adiabatic electrons is not well satisfied in the case of Deuterium ions, when $\sqrt{m_e/m_i} \sim 0.02 \approx 1^\circ$. Once $\phi_{DSE} < \phi_W$ it is no longer possible to assume that the Debye sheath repels most electrons back into the magnetic presheath — as is necessary for the electrons to be considered adiabatic — and the electron model becomes inaccurate. The critical value of α for which $\phi_{DSE} = \phi_W$

in the model increases slightly with τ : for $\tau = 2$ it is $\alpha \approx 3^\circ$, while for $\tau = 10$ it is $\alpha \approx 5^\circ$. (The expansion in $\alpha \ll 1$ is expected to break down for $\alpha > 5^\circ$, so results for these angles were not obtained.) In order to obtain an approximate form of the ion distribution function at the target for $\alpha \lesssim 3^\circ$ and $\tau \gtrsim 2 - 10$, the model presented here must be modified. A possible crude modification to the model is to set $v_c = 0$ and $\phi_{\text{DSE}} = \phi_{\text{W}}$ whenever the solution of equation (6.3) gives $\phi_{\text{DSE}} < \phi_{\text{W}}$. A more careful study, beyond the scope of this work, would be needed to solve the magnetic presheath and Debye sheath with a full kinetic model for the electrons.

8. Conclusions

The velocity distribution of ions reaching a planar target when the angle between the magnetic field and the target is small, $\alpha \ll 1$, was calculated using a model consisting of the set of equations (4.19), (4.21), (5.8), (6.3), (6.7), (6.13), (6.14) and (6.24) (replaced with (6.17) at the Debye sheath entrance instead of the target). The model, like the asymptotic theory it is based on, was argued to be valid for $\alpha \leq 5^\circ$. The advantage of the model is that the full solution of the quasineutrality equation in the magnetic presheath is bypassed, and replaced with constraints derived from quasineutrality near the Debye sheath entrance only. The treatment is more accurate for large ion gyro-orbits, $\tau = T_i/ZT_e \gg 1$, yet it can be used for $\tau \sim 1$ with qualitatively good results, as shown in figures 3, 6 and 7. Since the sputtering yield of an ion striking a target depends on the ion's energy and angle of incidence with the target, calculations of energy-angle distributions (7.11) using the model, shown in figures 6 and 7, may constitute a valuable resource for sputtering predictions.

The narrowing of the wall-normal velocity distribution with the angle α , shown in figure 3 at the Debye sheath entrance, is explained from the model as follows. Ions reaching the Debye sheath have a minimum normal velocity, $V_{x,\text{slow}}$, which depends on the size of the gyro-orbit, and so on the adiabatic invariant μ . Smaller gyro-orbits have a smaller gyration velocity and so a smaller magnetic force acts on the ion to maintain the gyro-motion, and a weaker electric force is needed to overcome the magnetic force and accelerate the ion towards the target. Ions in smaller gyro-orbits (smaller μ) are thus accelerated towards the wall for a larger distance, as shown schematically in figure 1(b-c). However, the dependence of $V_{x,\text{slow}}$ on the adiabatic invariant is weak, as seen in figure 4; thus, the distribution function quickly drops to zero below some small value of $|v_x|$, as seen in figure 3. The width of the wall-normal velocity distribution is therefore dominated by the gyrophase dependent piece of the ion velocity, giving the scaling $\langle \tilde{v}_x^2 \rangle \sim \alpha v_{t,i}^2$ for the variance of v_x .

The orderings (2.1) and (2.2) are required in the asymptotic theory and in the large gyro-orbit model, and are typically well-satisfied in fusion devices except for $\alpha \gg \sqrt{Zm_e/m_i}$ and $\rho_e \ll \lambda_D$. It will thus be crucial to understand the effect of non-adiabatic electrons, $\alpha \sim \sqrt{Zm_e/m_i}$, and of finite electron gyro-radius near the wall, $\rho_e \gtrsim \lambda_D$.

The author is grateful to Felix Parra for stimulating discussions and feedback. This work was supported by the US Department of Energy through grant DE-FG02-93ER-54197.

Appendix A. Change of $U_{\perp} - \chi_M(\bar{x})$ during the last ion gyro-orbit

In this appendix the change in the quantity $U_{\perp} - \chi_M(\bar{x})$ during the last gyro-orbit of an ion is calculated. This quantity is denoted $\Delta_M(\bar{x}, U)$, and is responsible for the spread of values of v_x in the ion distribution function at the Debye sheath entrance (5.9) and at the wall (5.10).

The rate of change of the quantity $U_{\perp} - \chi_M(\bar{x})$ is

$$\frac{d}{dt}(U_{\perp} - \chi_M) = \alpha \Omega^2 V_{\parallel}(x - x_M), \quad (\text{A } 1)$$

which is always positive for closed orbits which satisfy $x \geq x_b \geq x_M$. Consider an ion, at a position x , that has just reached values of \bar{x} and U_{\perp} such that $U_{\perp} = \chi_M(\bar{x})$. The time taken for the ion to reach $x = 0$ is approximated by integrating the equation $dx/dt = v_x \simeq \sigma_x \sqrt{2(\chi_M - \chi(0, \bar{x}))}$ to get

$$t = (\sigma_x + 1) \int_x^{x_t} \frac{dx}{\sqrt{2(\chi_M - \chi(x, \bar{x}))}} + \int_0^x \frac{dx}{\sqrt{2(\chi_M - \chi(x, \bar{x}))}}. \quad (\text{A } 2)$$

The problem with this approximation is that the second integral is logarithmically divergent due to the form of the integrand for $x \rightarrow x_M$ (recall that the effective potential maximum is always a stationary point with respect to x of the function $\chi(x, \bar{x})$ when the electrons are adiabatic),

$$\lim_{x \rightarrow x_M} \frac{1}{\sqrt{2(\chi_M - \chi(x, \bar{x}))}} = \frac{1}{\sqrt{\chi''(x_M) |x - x_M|}}. \quad (\text{A } 3)$$

However, the time t taken by an ion to reach the Debye sheath entrance from a point in its last gyro-orbit would only be infinite if $v_x = \sigma_x \sqrt{2(\chi_M - \chi(0, \bar{x}))}$ was exactly true. In practice, the quantity $U_{\perp} - \chi_M(\bar{x})$ is not exactly zero. To calculate this quantity, the time evolution of $U_{\perp} - \chi_M(\bar{x})$ is estimated in the same way the time t was estimated (incorrectly): we replace the time derivative in equation (A 1) with a spatial derivative using the substitution $d/dt = v_x d/dx$, and the approximation $v_x \simeq \sqrt{2(\chi_M - \chi(x, \bar{x}))}$ to obtain

$$\frac{d}{dx}(U_{\perp} - \chi_M) = \pm \alpha \Omega^2 V_{\parallel}(\chi_M(\bar{x}), U) \frac{x - x_M}{\sqrt{2(\chi_M - \chi(x, \bar{x}))}}. \quad (\text{A } 4)$$

This equation is then integrated in the same way as before to obtain

$$U_{\perp} - \chi_M(\bar{x}) = \alpha \Omega^2 V_{\parallel}(\chi_M(\bar{x}), U) \left[(\sigma_x + 1) \int_x^{x_{t,M}} \frac{s - x_M}{\sqrt{2(\chi_M - \chi(s, \bar{x}))}} ds + \int_0^x \frac{s - x_M}{\sqrt{2(\chi_M - \chi(s, \bar{x}))}} ds \right] \sim \left(\alpha + \frac{\alpha}{\tau} \right) c_s^2. \quad (\text{A } 5)$$

In equation (A 5) the size of $U_{\perp} - \chi_M$ is estimated as follows. For $\tau \gtrsim 1$, $V_{\parallel} \sim v_{t,i}$, $\sqrt{2(\chi_M - \chi(x, \bar{x}))} \sim v_{t,i}$ and $x_t - x_M \sim \rho_i$, giving $U_{\perp} - \chi_M \sim \alpha v_{t,i}^2 \sim \alpha c_s^2$. For $\tau \ll 1$, $V_{\parallel} \sim v_B$, and it was shown in Geraldini *et al.* (2019) that ion gyro-orbits grow in spatial extent while slowing down their gyro-motion to preserve adiabatic invariance, $\sqrt{2(\chi_M - \chi(x, \bar{x}))} \sim \tau v_B$ and $x_t - x_M \sim \rho_B$, giving $U_{\perp} - \chi_M \sim \alpha v_B^2 / \tau \sim \alpha c_s^2 / \tau$.

The second integral in (A 5) is not divergent near $x = x_M$ because the integrand tends to

$$\lim_{x \rightarrow x_M} \frac{x - x_M}{\sqrt{2(\chi_M - \chi(x, \bar{x}))}} = \frac{x - x_M}{\sqrt{\chi''(x_M) |x - x_M|}} = \Theta(x - x_M) \frac{1}{\sqrt{\chi''(x_M)}}, \quad (\text{A } 6)$$

which is always finite (moreover, the contribution from the region near $x = x_M$ in the integral (A 5) vanishes because the integrand changes sign there). Inserting the ordering from equation (A 5) into the equation $dx/dt = v_x \simeq \sigma_x \sqrt{2(\chi_M - \chi(x, \bar{x}))}$, we obtain an ordering for the time taken to reach $x = 0$,

$$t = (\sigma_x + 1) \int_x^{x_{t,M}} \frac{dx}{\sqrt{2(\chi_M - \chi(x, \bar{x})) + O((\alpha + \alpha/\tau)c_s^2)}} + \int_0^x \frac{dx}{\sqrt{2(\chi_M - \chi(x, \bar{x})) + O((\alpha + \alpha/\tau)c_s^2)}} = O\left(\frac{|\ln(\alpha + \alpha/\tau)|}{\Omega}\right). \quad (\text{A } 7)$$

The logarithmic contribution comes from the region near $x = x_M$, where the integrand tends to

$$\lim_{x \rightarrow x_M} \frac{1}{\sqrt{2(\chi_M - \chi(x, \bar{x}))}} = \frac{1}{\sqrt{\chi''(x_M)(x - x_M)^2 + O((\alpha + \alpha/\tau)c_s^2)}}. \quad (\text{A } 8)$$

Upper and lower bounds for the values of $U_\perp - \chi_M(\bar{x})$ of ions reaching $x = 0$ can be obtained using the fact that these ions must have past trajectories with a bottom bounce point x_b . We consider the following two limiting cases: (i) an ion crossing the maximum $x = x_M$ towards the sheath with $U_\perp = \chi_M(\bar{x}) + \epsilon$; (ii) an ion bouncing back (for the last time) from $x = x_M$ with $U_\perp = \chi_M(\bar{x}) - \epsilon$, where $\epsilon \ll \alpha(1 + 1/\tau)c_s^2$ is an energy difference so small it can be neglected. The minimum value of $U_\perp - \chi_M$ of an ion entering the Debye sheath is calculated from case (i),

$$U_\perp - \chi_M(\bar{x}) = -\Delta_+(x, \bar{x}, U), \quad (\text{A } 9)$$

where

$$\Delta_+(x, \bar{x}, U) = \alpha\Omega^2 V_{||}(\chi_M, U) \int_0^{x_M} \frac{x_M - s}{\sqrt{2(\chi_M - \chi(x, \bar{x}))}} \quad (\text{A } 10)$$

is a positive quantity. The maximum value of $U_\perp - \chi_M(\bar{x})$ is calculated from case (ii),

$$U_\perp - \chi_M(\bar{x}) = \Delta_M(\bar{x}, U) - \Delta_+(x, \bar{x}, U), \quad (\text{A } 11)$$

where

$$\Delta_M(\bar{x}, U) = 2\alpha\Omega^2 V_{||}(\chi_M, U) \int_{x_M}^{x_t} \frac{s - x_M}{\sqrt{2(\chi_M - \chi(x, \bar{x}))}}. \quad (\text{A } 12)$$

Equation (4.22) follows from the equality

$$\mu'_{\text{op}}(\bar{x}) = \Omega^2 \int_{x_M}^{x_t} \frac{s - x_M}{\sqrt{2(\chi_M - \chi(x, \bar{x}))}}, \quad (\text{A } 13)$$

which can be verified from (4.20). The quantity Δ_+ was shown to be negligible when calculating v_x from equation (4.12), as it is always small relative to either $\chi_M(\bar{x}) - \chi(x, \bar{x})$ or $\Delta_M(\bar{x}, U)$ (Geraldini *et al.* 2018).

Appendix B. Ion conservation

The ion distribution function at the Debye sheath entrance, equation (5.9), is proved here to be consistent with ion conservation in the magnetic presheath. Equation (5.5) gives the current flowing normal to the wall at the magnetic presheath entrance. In steady state, the current flowing normal to the wall at the Debye sheath entrance should be the

same. At the Debye sheath entrance, the ion density is small in α and the ion current flowing normal to the wall is due to the component v_x of the the velocity of all ions,

$$\frac{j_{i,x}}{Ze} = -2\pi \int_{\bar{x}_c}^{\infty} \Omega d\bar{x} \int_{\Omega\mu}^{\infty} \frac{F(\mu_{\text{op}}(\bar{x}), U) dU}{V_{\parallel}(\chi_{\text{M}}(\bar{x}), U)} \quad (\text{B1})$$

$$\times \int_{-\infty}^{\infty} \hat{H} \left(\frac{1}{2} v_x^2 - \chi_{\text{M}}(\bar{x}) + \frac{1}{2} \Omega^2 \bar{x}^2 + \frac{\Omega \phi_{\text{DSE}}}{B}, 0, \Delta_{\text{M}}(\bar{x}, U) \right) v_x dv_x \quad (\text{B2})$$

The last integral in v_x is taken by replacing $v_x dv_x = d(v_x^2/2)$, and the result is $\Delta_{\text{M}}(\bar{x}) = 2\alpha\pi\mu'_{\text{op}}(\bar{x})V_{\parallel}(\chi_{\text{M}}(\bar{x}), U)$,

$$\frac{j_{i,x}}{Ze} = -2\alpha\pi \int_0^{\infty} \Omega d\bar{x} \mu'_{\text{op}}(\bar{x}) \int_{\Omega\hat{\mu}}^{\infty} F(\mu, U) dU. \quad (\text{B3})$$

Using $\mu'_{\text{op}}(\bar{x}) = d\mu/d\bar{x}$ and changing integration variable to μ leads to equation (5.5). The same argument straightforwardly applies to the ion distribution function at the wall, (5.10), and to the large gyro-orbit model distribution functions, (6.17) and (6.24).

REFERENCES

- ANDERS, A., ANDERS, S. & BROWN, I. G. 1995 Transport of vacuum arc plasmas through magnetic macroparticle filters. *Plasma Sources Science and Technology* **4** (1), 1.
- BAALRUD, S. & HEGNA, C. 2012 Reply to comment on kinetic theory of the presheath and the bohm criterion. *Plasma Sources Science and Technology* **21** (6), 068002.
- BAALRUD, S. D., SCHEINER, B., YEE, B., HOPKINS, M. M. & BARNAT, E. 2019 Interaction of biased electrodes and plasmas: Sheaths, double layers and fireballs , arXiv: 1911.06424.
- BOEUF, J.-P. 2017 Tutorial: Physics and modeling of hall thrusters. *Journal of Applied Physics* **121** (1), 011101.
- BORODKINA, I., BORODIN, D., KIRSCHNER, A., TSVETKOV, I., KURNAEV, V., KOMM, M., DEJARNAC, R. & CONTRIBUTORS, J. 2016 An analytical expression for the electric field and particle tracing in modelling of be erosion experiments at the jet iter-like wall. *Contributions to Plasma Physics* **56** (6-8), 640–645.
- CHODURA, R. 1982 Plasma–wall transition in an oblique magnetic field. *Physics of Fluids (1958-1988)* **25** (9), 1628–1633.
- COHEN, R. H. & RYUTOV, D. D. 1998a Particle trajectories in a sheath in a strongly tilted magnetic field. *Physics of Plasmas (1994-present)* **5** (3), 808–817.
- COHEN, R. H. & RYUTOV, D. D. 1998b Sheath over a rough surface in a tilted magnetic field. *Physics of Plasmas* **5** (6), 2194–2196.
- COULETTE, D. & MANFREDI, G. 2016 Kinetic simulations of the chodura and debye sheaths for magnetic fields with grazing incidence. *Plasma Physics and Controlled Fusion* **58** (2), 025008.
- DROBNY, J., HAYES, A., CURRELI, D. & RUZIC, D. N. 2017 F-tridyn: A binary collision approximation code for simulating ion interactions with rough surfaces. *Journal of Nuclear Materials* **494**, 278–283.
- GERALDINI, A., PARRA, F. I. & MILITELLO, F. 2017 Gyrokinetic treatment of a grazing angle magnetic presheath. *Plasma Physics and Controlled Fusion* **59** (2), 025015.
- GERALDINI, A., PARRA, F. I. & MILITELLO, F. 2018 Solution to a collisionless magnetic presheath with kinetic ions. *arXiv preprint arXiv:1805.02975* .
- GERALDINI, A., PARRA, F. I. & MILITELLO, F. 2019 Dependence on ion temperature of shallow-angle magnetic presheaths with adiabatic electrons. *Journal of Plasma Physics* **85** (6), 795850601.
- GUNN, J., CARPENTIER-CHOUGHANA, S., DEJARNAC, R., ESCOURBIAC, F., HIRAI, T., KOMM, M., KUKUSHKIN, A., PANAYOTIS, S. & PITTS, R. 2017 Ion orbit modelling of elm heat loads on iter divertor vertical targets. *Nuclear Materials and Energy* **12**, 75–83.
- HASTINGS, D. 1995 A review of plasma interactions with spacecraft in low earth orbit. *Journal of Geophysical Research: Space Physics* **100** (A8), 14457–14483.

- HERSHKOWITZ, N. 2005 Sheaths: More complicated than you think. *Physics of plasmas* **12** (5), 055502.
- HUTCHINSON, I. H. 2002 Principles of plasma diagnostics. *Plasma Physics and Controlled Fusion* **44** (12), 2603.
- KHAZIEV, R. & CURRELI, D. 2015 Ion energy-angle distribution functions at the plasma-material interface in oblique magnetic fields. *Physics of Plasmas (1994-present)* **22** (4), 043503.
- KRASHEINNIKOV, S. & KUKUSHKIN, A. 2017 Physics of ultimate detachment of a tokamak divertor plasma. *Journal of Plasma Physics* **83** (5).
- LASA, A., CANIK, J., BLONDEL, S., YOUNKIN, T., CURRELI, D., DROBNY, J., ROTH, P., CIANCIOSA, M., ELWASIF, W., GREEN, D. & OTHERS 2020 Multi-physics modeling of the long-term evolution of helium plasma exposed surfaces. *Physica Scripta* **2020** (T171), 014041.
- LOIZU, J., RICCI, P., HALPERN, F. D. & JOLLIET, S. 2012 Boundary conditions for plasma fluid models at the magnetic presheath entrance. *Physics of Plasmas (1994-present)* **19** (12), 122307.
- MILITELLO, F. & FUNDAMENSKI, W. 2011 Multi-machine comparison of drift fluid dimensionless parameters. *Plasma Physics and Controlled Fusion* **53** (9), 095002.
- MOSETTO, A., HALPERN, F. D., JOLLIET, S., LOIZU, J. & RICCI, P. 2015 Finite ion temperature effects on scrape-off layer turbulence. *Physics of Plasmas* **22** (1), 012308.
- PARKS, P. B. & LIPPMANN, S. I. 1994 Effect of magnetic field on the distribution of ions striking a planar target. *Physics of Plasmas* **1** (12), 3883–3889.
- RIEMANN, K.-U. 1991 The Bohm criterion and sheath formation. *Journal of Physics D: Applied Physics* **24** (4), 493.
- RIEMANN, K.-U. 2012 Comment on kinetic theory of the presheath and the bohm criterion. *Plasma Sources Science and Technology* **21** (6), 068001.
- SIDDIQUI, M. U., THOMPSON, D. S., JACKSON, C. D., KIM, J. F., HERSHKOWITZ, N. & SCIME, E. E. 2016 Models, assumptions, and experimental tests of flows near boundaries in magnetized plasmas. *Physics of Plasmas (1994-present)* **23** (5), 057101.
- STANGEBY, P. C. 2000 *The plasma boundary of magnetic fusion devices* (IOP publishing, Bristol, UK) .
- STANGEBY, P. C. 2012 The chodura sheath for angles of a few degrees between the magnetic field and the surface of divertor targets and limiters. *Nuclear Fusion* **52** (8), 083012.
- TSKHAKAYA, D. & KUHN, S. 2003 Particle-in-cell simulations of the plasma-wall transition with a magnetic field almost parallel to the wall. *Journal of nuclear materials* **313**, 1119–1122.